JBC RESEARCH ARTICLE

Kinetic complexities of triacylglycerol accumulation in developing embryos from *Camelina sativa* provide evidence for multiple biosynthetic systems

Received for publication, August 13, 2021, and in revised form, October 28, 2021 Published, Papers in Press, November 12, 2021,
https://doi.org/10.1016/j.jbc.2021.101396

Mike Pollard and Yair Shachar-Hill*

From the Department of Plant Biology, Michigan State University, East Lansing, Michigan, USA

Edited by Dennis Voelker

Quantitative flux maps describing glycerolipid synthesis can be important tools for rational engineering of lipid content and composition in oilseeds. Lipid accumulation in cultured embryos of *Camelina sativa* is known to mimic that of seeds in terms of rate of lipid synthesis and composition. To assess the kinetic complexity of the glycerolipid flux network, cultured embryos were incubated with [$^{14}C/^{13}C$]glycerol, and initial and steady state rates of [$^{14}C/^{13}C$*glyceryl*] lipid accumulation were measured. At steady state, the linear accumulations of labeled lipid classes matched those expected from mass compositions. The system showed an apparently simple kinetic precursor–product relationship between the intermediate pool, dominated by diacylglycerol (DAG) and phosphatidylcholine (PC), and the triacylglycerol (TAG) product. We also conducted isotopomer analyses on hydrogenated lipid class species. [$^{13}C_3$*glyceryl*] labeling of DAG and PC, together with estimates of endogenous [$^{12}C_3$*glyceryl*] dilution, showed that each biosynthetically active lipid pool is ∼30% of the total by moles. This validates the concept that lipid sub-pools can describe lipid biosynthetic networks. By tracking the kinetics of [$^{13}C_3$*glyceryl*] and [$^{13}C_2$*acyl*] labeling, we observed two distinct TAG synthesis components. The major TAG synthesis flux (∼75%) was associated with >95% of the DAG/PC intermediate pool, with little glycerol being metabolized to fatty acids, and with little dilution from endogenous glycerol; a smaller flux exhibited converse characteristics. This kinetic heterogeneity was further explored using postlabeling embryo dissection and differential lipid extractions. The minor flux was tentatively localized to surface cells across the whole embryo. Such heterogeneity must be recognized in order to construct accurate gene expression patterns and metabolic networks describing lipid biosynthesis in developing embryos.

Oilseed crops supply vegetable oils for food, nutrition, cosmetic, and industrial product markets. Triacylglycerols (TAGs) are the dominant storage lipids in the oil (typically ≥98 mol%), whereas diacylglycerols (DAGs), lecithin, sterols, and tocopherols are minor constituents. Oils with unique fatty acid and lipid structures are destined for specialized end uses. Examples include castor for the production of ricinoleate-rich oils for oleochemical uses (1) and transgenic crops engineered to produce eicosapentaenoic and docosahexaenoic acids for the nutritional supplement market (2). Considerable effort has been directed at gene engineering of commercial oilseeds to produce novel plant oils (3–6). One goal has been to reproduce novel oil compositions found across the plant kingdom. This has generally met with only partial success, in that novel fatty acids have indeed been introduced but usually not at levels to warrant commercial development. Attempts to substantially increase oil content through genetic engineering have apparently not resulted in commercial lines, despite many claims of success in the laboratory. Against this backdrop, a deeper understanding of metabolism is required as an adjunct to simply isolating and expressing sets of genes observed to be highly expressed in plant tissues producing elevated or novel oils.

The complexities of seed fatty acid and lipid synthesis, including metabolic pathways, enzymes and genes, subcellular localization, and regulation, have been thoroughly reviewed elsewhere (7, 8). Briefly, and pertinent to this work, is that cytosolic glycerol-3-phosphate (G3P) is acylated to give phosphatidic acid. This intermediate does not accumulate to any significant degree but is hydrolyzed to *sn*-1,2-DAG. DAG is converted or interconverted to phosphatidylcholine (PC) by several mechanisms, with PC being the substrate for acyl desaturation. TAG can be synthesized directly *via* the acyl-CoA-dependent *sn*-3 acylation of DAG by diacylglycerol acyltransferases (DGAT1 or DGAT2) or by a transacylation reaction between PC and DAG catalyzed by phospholipid diacylglycerol acyltransferase (PDAT), with regeneration of 1-acyl-lyso-PC to PC catalyzed by acyl-CoA:lyso-PC acyltransferase. And finally, TAG is sequestered into oil bodies (9). An important feature is that membrane lipid synthesis shares many of the same enzyme reactions with neutral lipid synthesis. Thus, for seeds that have evolved unique fatty acid compositions, and also neutral lipid end products besides TAG, there must have occurred substantial coevolution of two distinctive lipid synthesis processes, especially when high levels of a novel end product are accumulated. Membrane biogenesis and homeostasis in the plant cell cannot be adversely perturbed.

* For correspondence: Yair Shachar-Hill, yairhill@msu.edu.

This is probably the broad underlying reason that has limited many attempts to genetically engineer lipid composition.

An attempt to quantify acylglycerolipid metabolism was carried out using immature soybean (*Glycine max*) embryos (10). The study tracked initial rates using [^{14}C] acetate and glycerol as substrates. Kinetic data were combined with compositional analysis to derive a quantitative flux map. This was apparently the first attempt at flux mapping of lipid metabolism in oilseeds and must be regarded as the first draft in the continuing improvement and refinement of such models. The modeling required several assumptions, two of which are that (i) "the cells are in a relatively uniform physiological state" and (ii) "although exogenous "nonphysiological" substrates may penetrate differently and may perturb metabolism slightly differently, they effectively report the bulk tissue metabolism." In addition to labeling kinetics combined with analyses of lipid molecular species applied to mutant and transgenic lines, to generate models, the intervening time has seen the proliferation of methods to measure protein–protein interactions for lipid enzymes (11, 12). These methods are being applied to oilseeds (13, 14), resulting in the proposal of metabolons to describe metabolism. However, measuring protein–protein interactions without solid evidence for metabolite channeling provides insufficient evidence for a metabolon (12).

Camelina sativa is currently grown as a niche oilseed crop to produce oil for biofuel. Its seed oil is rich in oleic, linoleic, linolenic, and eicosenoic acids. Camelina is also used as a model system for oilseed applications research, with focus on enhancing seed yield, oil content, and the accumulation of unusual fatty acids (2, 15–19). This research has been augmented by multiple studies on the Camelina transcriptome, characterizations of lipid biosynthetic enzymes (20, 21), and flux mapping of embryo central carbon metabolism excluding lipids (22). The availability of a quantitative flux map for acylglycerol lipid biosynthesis in developing Camelina embryos will add to the useful tools for the design and analysis of seed genetic engineering experiments. To this end, the ability of cultured developing embryos of *C. sativa* to replicate *in vivo* seed lipid metabolism has been confirmed (23), while the optimized use and potential limitations of acetate and glycerol as substrates for isotopic labeling were reported (24). Although flux maps for central carbon metabolism are determined by flux balance and metabolic flux analysis, kinetic labeling analysis is needed to elucidate lipid metabolism. These approaches assume uniform patterns of flux in the steady state condition, but unrecognized tissue heterogeneity may modulate or even invalidate any quantitative network map produced. In common with other Brassicaceae, heterogeneity of lipid composition has been measured by MALDI–MS imaging of mature Camelina seeds (25). Most noteworthy were the preferential accumulation of C56 TAG in the cotyledons and C54 TAG in the axis. The C56 TAGs contain a C20 fatty acid, predominantly eicosenoic acid. This and other C20–C24 very long-chain fatty acids (VLCFAs) are synthesized *via* the action of cytoplasmic fatty acyl-CoA elongase (FAE1) (26). An additional source of embryo heterogeneity, differential cotyledon development caused by seed architecture, has also been noted (27).

Our strategy for developing a quantitative Camelina seed lipid flux map has been to lead with wildtype, in part because use of mutants, although ideal for identification of contributing enzymes and genes, may not provide the baseline flux map as compensatory metabolic mechanisms kick in. Second, assays with embryos are much preferred over whole seeds. In seeds from the Brassicaceae, the embryo typically provides 85 to 90% of the seed oil content (28). Of course, the embryo is a whole plant, with a complexity of cell types (29), but the assay of seeds will confound simple substrate uptake because of multiple entry routes through the injured vasculature of the funiculus and *via* the seed coat. In addition, multiple seed coat layers and endosperm may concentrate and complicate labeling. A metabolic flux map describing glycerolipid biosynthesis must track glyceryl (lipid glycerol backbone) and acyl fluxes, plus any glyceryl head group interconversions. By definition, tracking the interconversion of glyceryl fluxes through lipid classes will define a subset of acyl fluxes. Layered onto this will be sets of acyl editing fluxes while building further complexity will include acyl group and lipid acyl carbon number and degree of desaturation, and finally full stereochemical analysis. This work is focused primarily on glyceryl fluxes as the first level in model building. Because of the high rate of glyceryl labeling provided by exogenous glycerol in culture (24), [$^{13}C_3$]glycerol labeling has been combined with [U-^{14}C]glycerol labeling. Some glycerol label is diverted into acyl metabolism. To distinguish between glyceryl and acyl labeling, [$^{13}C_n$] lipid isotopomer analysis by MS was employed.

Lipid glyceryl labeling over both short and long durations allowed measurement of initial and steady state rates of product accumulation, respectively. The overall labeling kinetics were characteristic of a precursor–product kinetic system and showed product accumulation rates that mimicked the *in vivo* situation. As expected for oilseeds rich in polyunsaturated fatty acids, initial labeling of glyceryl backbones was predominantly in DAG and PC (30). [$^{13}C_3$*glyceryl*] labeling, when combined with an estimate of endogenous [$^{12}C_3$*glyceryl*] dilution, showed that for both DAG and PC, the biosynthetically active pool is ∼30 mol% of the total embryo amount. Flux modeling often invokes multiple pools of a metabolite to describe the network more exactly (31). The results for PC and DAG confirm that kinetically distinct pools exist for these core lipid classes. The biological possibilities that might account for lipid pools that are active or largely inactive in *de novo* glycerolipid synthesis are discussed.

Because exogenous glycerol labels both the glyceryl backbone and acyl groups of lipids, to produce [$^{13}C_3$*glyceryl*] and [$^{13}C_{2n}$*acyl*] isotopomers, respectively, the analytical method employed must be able to distinguish these possibilities. By tracking the kinetics of these labeling patterns, at least two distinct TAG synthesis components were observed. The major

TAG synthesis flux was associated with large DAG and PL intermediate pools, with little glycerol metabolized to fatty acid synthesis precursors, and with little dilution from endogenous glycerol. The minor TAG producing system(s) showed the converse attributes. Although this study began with the assumption that glycerol substrate would be utilized by the embryo in a relatively uniform manner, the kinetic heterogeneity uncovered must be recognized in order to construct accurate metabolic networks to describe lipid biosynthesis in developing embryos. The multiple TAG synthesis systems are associated neither with differences (such as expression of FAE1) between the axis and cotyledons nor by the differential development of the inner and outer cotyledons but are most likely a function of different carbon and lipid metabolism in the outermost layer(s) of the embryo *versus* the inner cell layers.

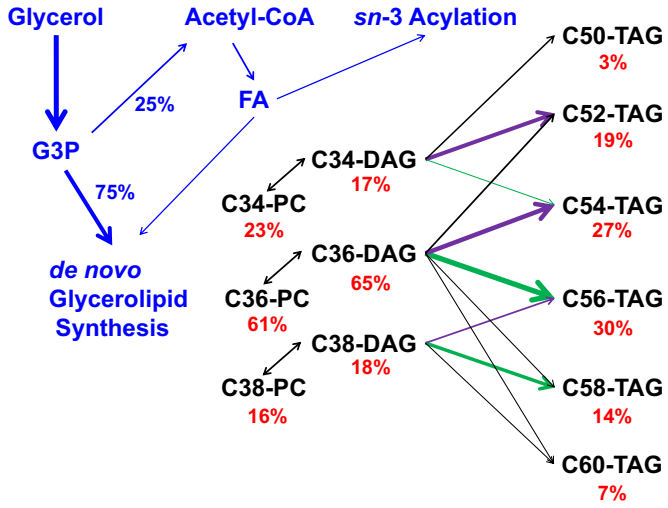

Figure 1. Interrelationships between lipid molecular species and flow of label from glycerol. The production of different TAG acyl carbon number molecular species from PC and DAG, as deduced from ESI–MS analysis of hydrogenated lipid products after culturing Camelina embryos with a mixture of [U-^{14}C] and [$^{13}C_3$]glycerol, is shown. Most of the glycerol (in *blue*) is incorporated into acylglycerolipid backbones, but about 25 mol% is utilized for fatty acid synthesis. The values in *red* are molar % mass distributions (n = 3) within each lipid class at 24 h culture. The likely major and minor biosynthetic fluxes are shown. These are estimated based on the TAG molecular species compositions and the assumption that DAG pool sizes are commensurate with the flux from DAG to TAG. The *colored arrows* represent major fluxes for *sn*-3 acylation with C18 fatty acids (*purple*) and C20 fatty acids (*green*). *Arrow* thicknesses highlight the relative fluxes from each DAG class to TAG. Table S1 provides additional information. DAG, diacylglycerol; ESI, electrospray ionization; PC, phosphatidylcholine; TAG, triacylglycerol.

Results

Overview of glycerol labeling and ^{13}C lipid isotopomer analysis

Exogenous glycerol primarily labels the glyceryl backbone of acyl lipids, but some labeling of fatty acids also occurs, as shown for Camelina embryos (24), soybean embryos (10), and maize leaves (32). Thus, dual utilization is likely a general phenomenon in plants. After uptake, glycerol is phosphorylated to provide G3P to initiate glycerolipid synthesis. In addition, in the process of generating acetyl-CoA from G3P for fatty acid synthesis, one ^{14}C or ^{13}C label is lost from uniformly labeled glycerol. The kinetic experiments reported here utilized a mixture of [U-^{14}C]glycerol and [$^{13}C_3$]glycerol substrates. The radioactive tracer was used to quantify moles of exogenous glycerol incorporated into different lipid classes separated by TLC. The division of glycerol label between acyl and glyceryl moieties complicates analysis. For ^{14}C labeling, total lipids or lipid classes can be transmethylated, and the hexane-extractable label (fatty acid methyl esters) can be measured to give the acyl-labeled fraction, whereas the aqueous phase contains the glyceryl label. However, MS of glycerolipids with ^{13}C isotopomer analysis provides extra information in that the connectivities between acyl and glyceryl labeling can also be measured. This additional information has proven useful, and the isotopomer method has been used for all the data presented in this article. In the next section, a comparison between the ^{14}C transmethylation method and the mass spectroscopy ^{13}C isotopomer method is briefly described. There is reasonable agreement between the two.

Unraveling the complex molecular ion profiles obtained by mass spectroscopy of intact acyl lipids is made even more difficult by ^{13}C labeling. To circumvent this problem, the lipid samples were fully hydrogenated prior to TLC separation and electrospray ionization (ESI)–MS analysis (23, 24). This greatly simplifies the molecular ion profiles for each C_n lipid, allowing deconvolution of biosynthetic ^{13}C isotopomer profiles. The C_n species, as defined by the total number of acyl carbon atoms, of TAG, DAG, and PC analyzed by ESI–MS are shown in Figure 1. C_n molecular species molar distributions over a 4-day culture period are listed in Table S1. Although these C_n distributions change little over time, molecular species as defined by unsaturation will change since the ratio of linolenate to linoleate increases significantly over the culture period (24). DAG and PC C_n distributions are similar (Fig. 1). This is consistent with their similar fatty acid compositions (23) and with biosynthetic models that propose a major reversible head-group exchange flux between active DAG and PC pools (33–36). The acyl compositions are (C16 + C18) for C34, (C18 + C20) for C38, and predominantly (C18 + C18) for the major C36 species, with a very minor (≤3 mol% of C36 total) contribution from (C16 + C20). Also shown are conversions of DAGs to TAGs, with the expected *sn*-3 acylations by specific fatty acids (with C18 in *purple* and C20 in *green* to aid in identification); and ∼3:1 M ratio for glyceryl *versus* acetyl utilization from exogenous glycerol at steady state.

Details of MS ^{13}C isotopomer analysis of hydrogenated and purified TAG, DAG, and PC lipid classes are given in "Supplemental text for ^{13}C isotopomer analysis" of the supporting information and Figures S1–S4. In summary, the level of glycerol labeling of fatty acids when compared with lipid glyceryl labeling was such that only (M + 2), (M + 3), and (M + 5) biosynthetic isotopomers (corresponding to [$^{13}C_2$*acyl*], [$^{13}C_3$*glyceryl*], and [$^{13}C_5$*acyl* + *glyceryl*] labeling respectively, Fig. S1) were formed to a significant degree. In addition, unlike acetate (23, 24, 37–39), acyl labeling from glycerol did not

preferentially label VLCFAs (Fig. S2). And finally, a worked example of an isotopomer calculation, for C36-PC, is provided (Fig. S3).

Glyceryl kinetic steady state labeling suggests a simple precursor–product model

Figure 2 shows the incorporation of exogenous glycerol into [$^{13/14}$C-*glyceryl*] total lipids and individual lipid classes over a 96 h period. Two methods were assessed in order to correct for [$^{13/14}$C-*acyl*] labeling of lipids that occurs concurrently with [$^{13/14}$C-*glyceryl*] labeling (Fig. S4*A*). Transmethylation analysis of [^{14}C] total lipids gave hexane-extractable products ranging from 11.5 to 15.5% of total radioactivity, similar to values reported previously (24). The ^{13}C isotopomer calculation produced values of 14.5 to 18%. There was a noticeable reduction in acyl labeling over 8 to 24 h, consistent across both methods, and confirmed in a second short-term kinetic experiment (Fig. S4*A*). It is worth noting that the labeled acyl contribution is a cumulative average over the assay period. Its value varied modestly. Despite some modulation in acyl *versus* glyceryl labeling over 8 to 96 h on average, about 75 mol% of glycerol incorporated was converted to lipid glyceryl groups and 25 mol% to lipid acyl groups (Fig. S4, *B* and *C*). The mass of fatty acids recovered after transmethylation of the hydrogenated total lipid samples showed an acceleration of lipid accumulation rate, such that the rate after 4 days was twofold greater than initially (Fig. S4*D*). This is consistent with previous observations on extended culturing of midmaturation embryos (23, 24). The estimated initial and final net glyceryl lipid synthesis rates from fatty acid mass measurements were 1.54 and 3.205 nmol/h/embryo, respectively.

The steady state rates and intercepts from Figure 2 for total lipids and lipid classes are listed in Table 1. The time course produced a linear rate of 1.22 nmol/h/embryo for incorporation of exogenous glycerol into [*glyceryl*] total lipids, a value in line with previous assays of glycerol incorporation at saturating

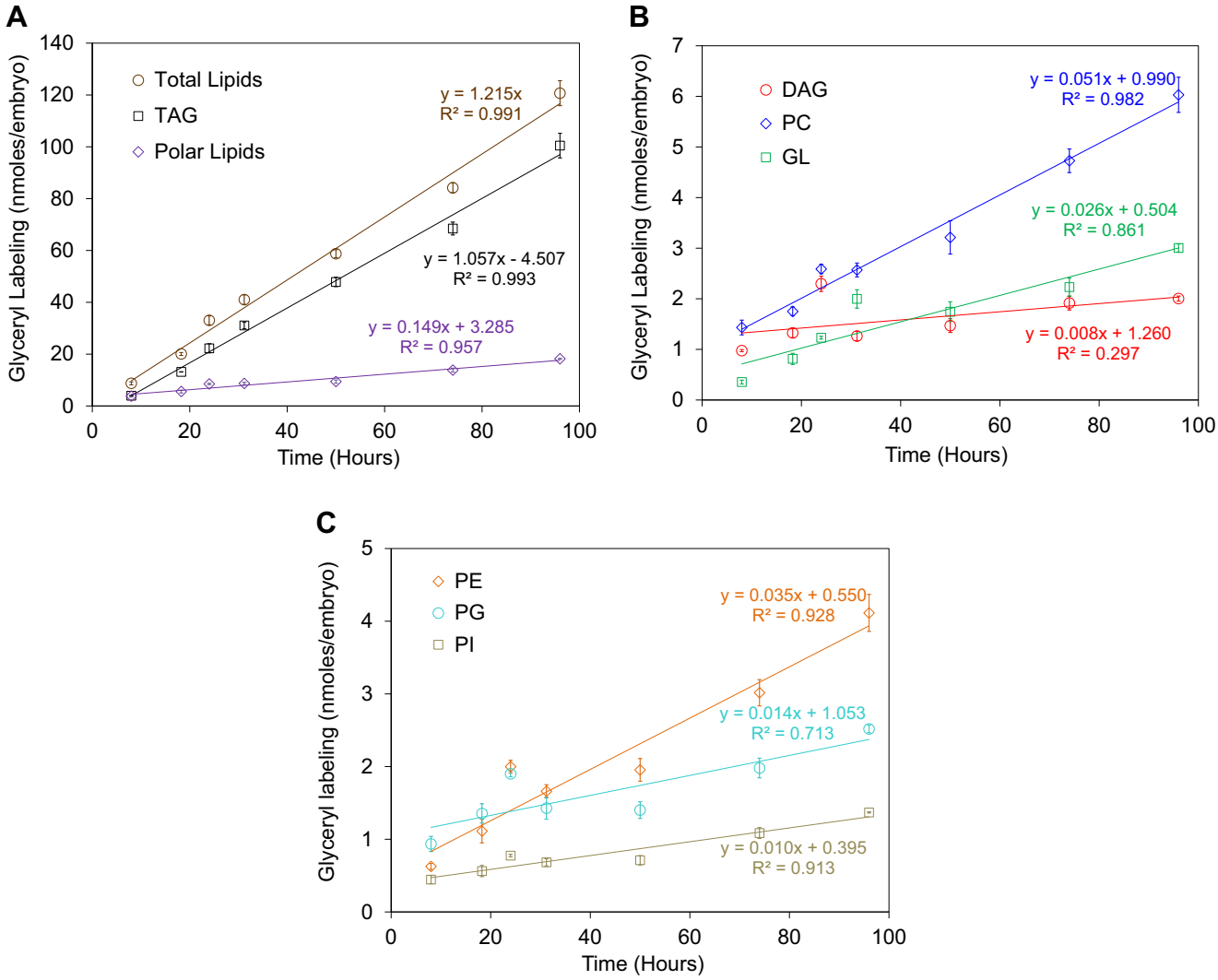

Figure 2. Glyceryl labeling of total lipids and lipid classes over a 4-day culture period. *A–C*, assays were run at 2 mM total glycerol (tracer amount of [$^{14}C_3$]glycerol with the remainder as [$^{13}C_3$]glycerol) over a 4-day period. Glyceryl labeling reports the sum of ^{14}C plus ^{13}C labeling and was estimated using the ^{13}C isotopomer calculation protocol. The equation and r^2 value for the best-fit linear fit are also given. Error bars denote ±SD (n = 3).

Table 1
Steady state rates of synthesis and precursor pool size estimates derived from kinetic assays

Lipid	Slope (nmol/h/embryo)	Intercept (nmol/embryo)	16 DPA zygotic Embryos[a] (mole acyl groups, %)
Total	1.215 (100%)		
TAG	1.057 (87%)	−4.51	89%[a]
DAG	0.008 (0.7%)	+1.26	1.2%
PL	0.149 (12.3%)	+3.28	9.8%
Sum	1.215	+4.54, −4.51	
PC	0.051 (4.2%)	+0.99	4.4%
PE	0.036 (3.0%)	+0.56	0.7%
PI	0.009 (0.75%)	+0.41	0.25%
PG	0.014 (1.15%)	+1.06	0.8%
GL(**)	0.025 (2.1%)	+0.49	2.15%
Sum	0.135	+3.51	8.3%

Summary of steady state rates and intercepts from Figure 2 for total lipids and lipid classes.
[a] For comparison, the distribution of lipids (as moles of acyl groups) measured in 16 DPA zygotic embryos is presented (23). TAG includes molecular species containing at least one acyl group with an epoxy or hydroxy functional group.

concentrations, which gave 1.48 ± 0.35 nmol/h/embryo (n = 6) (24). The results showed that the steady state accumulation rates of end products matched the expected lipid class composition. The steady state linear accumulations of end products were 87.4 mol% TAG, 0.7 mol% DAG, and 11.8 mol% polar lipid (PL, mainly phospholipids plus galactolipids). If the mole % glycerol incorporated into TAG is 87%, 91% of acyl groups will be esterified into TAG. An important observation was that pools such as individual PLs were growing. This can be interpreted as (i) expansion of biosynthetically active intermediate pools, (ii) shunting into end product pools that accumulate without turnover, and/or (iii) replacement of any endogenous PL.

Glycerol incorporation into [^{14}C/^{13}C-*glyceryl*] total lipids was linear (Fig. 2*A*). The line of best fit, $y = 1.215 + 0.260$ (r^2 = 0.993), was statistically indistinguishable from a zero intercept line of the same slope. Thus, any lag between exposure to labeled glycerol and its incorporation into lipids is very short. The best-fit straight lines are also shown for total TAG, that is, TAG that may include epoxy and hydroxy acyl groups (23), and for total PL. Neither passed through the origin. As shown theoretically in the supporting information (Fig. S5), an *x*-intercept correlates to the time to fill an intermediate pool and the *y*-intercept to the pool size. As the labeling of TAG, the major end product, was linear from the first time point onward (8 h), the system must be in kinetic steady state with respect to labeling over the measurement period, and intermediate pool filling must take $<<$8 h. In fact, the pool filling time (occurring when $y = 0$; Figs. 2*A* and S5) was calculated as 4.26 h. Thus, the half-life for filling the TAG precursor pool in this experiment was 2.95 h.

PL and DAG provide the intermediate glycerolipid pool for TAG synthesis. Labeled PL accumulation is shown in Figure 2*A*, whereas DAG, PC, phosphatidylethanolamine (PE), phosphatidylglycerol (PG), phosphatidylinositol (PI), and monogalactosyldiacylglycerol and digalactosyldiacylglycerols (galactolipids [GLs]) are shown in Figure 2, *B* and *C*. The radioactivity in these lipid classes, as a percentage of total radioactivity, ranged from 14% for PC and 10% for DAG at 8 h, down to 1 to 4.5% levels at 4 days. All the lipid classes gave good straight line fits for glyceryl labeling. As shown in Table 1, the sum of steady state rates for TAG + DAG + PL is very close to the rate for total lipid accumulation. The sum of PC + PE + PI + PG + GL rates (0.135 nmol/h/embryo) accounts for most (89%) of the PL labeling (0.149 nmol/h/embryo). As noted previously, the intersection of the line for TAG accumulation on the *x*-axis gave the turnover time for the total precursor pool providing TAG synthesis as 4.26 h. TAG represented 1.057/1.215 = 87% of the total end product flux from this metabolically active lipid pool. The linear rate of TAG accumulation extrapolated back to the *y*-intercept at −4.51 nmol/embryo. Thus, the precursor pool, which supplied TAG and other lipids, is estimated at 4.51 × 1.215/1.057 = 5.18 nmol/embryo. Combining the DAG + PL linear rates of accumulation gave 0.1494 + 0.0081 = 0.1575 nmol/h/embryo for end product accumulations. The corresponding summed intercept value is 4.54 nmol, so correction gives 4.54 × 1.215/1.057 = 5.22 nmol/embryo as another estimate of the total turnover pool size. These precursor pool estimates are therefore consistent with each other, and thus, a simple precursor–product kinetic model is adequate to describe the overall system. That is, labeling kinetics demonstrate that TAG synthesis is completely integrated with *de novo* biosynthesis of membrane glycerolipids. That does not rule out additional complexity within the precursor pool on a time scale equal to or less than that of the pool filling time.

Initial rates of glyceryl lipid class labeling are dominated by DAG and PC synthesis

To complement the longer kinetic experiment showing linear rates (Fig. 2), a shorter term glycerol labeling experiment (0.4–22 h) was undertaken to track initial rates and precursor–product relationships preceding the steady state condition (Figs. 3 and S6). The incorporation of [$^{13/14}$C]glycerol into [$^{13/14}$C*glyceryl*] total lipids was linear (1.06 nmol/h/embryo, r^2 = 0.991), whereas TAG accumulation exhibited a lag phase and DAG + PL show filling of the intermediate pool and accompanying steady state accumulation (Fig. 3*A*). It is not possible to measure steady state rates with the accuracy and statistical precision achieved in Figure 2, since there are a

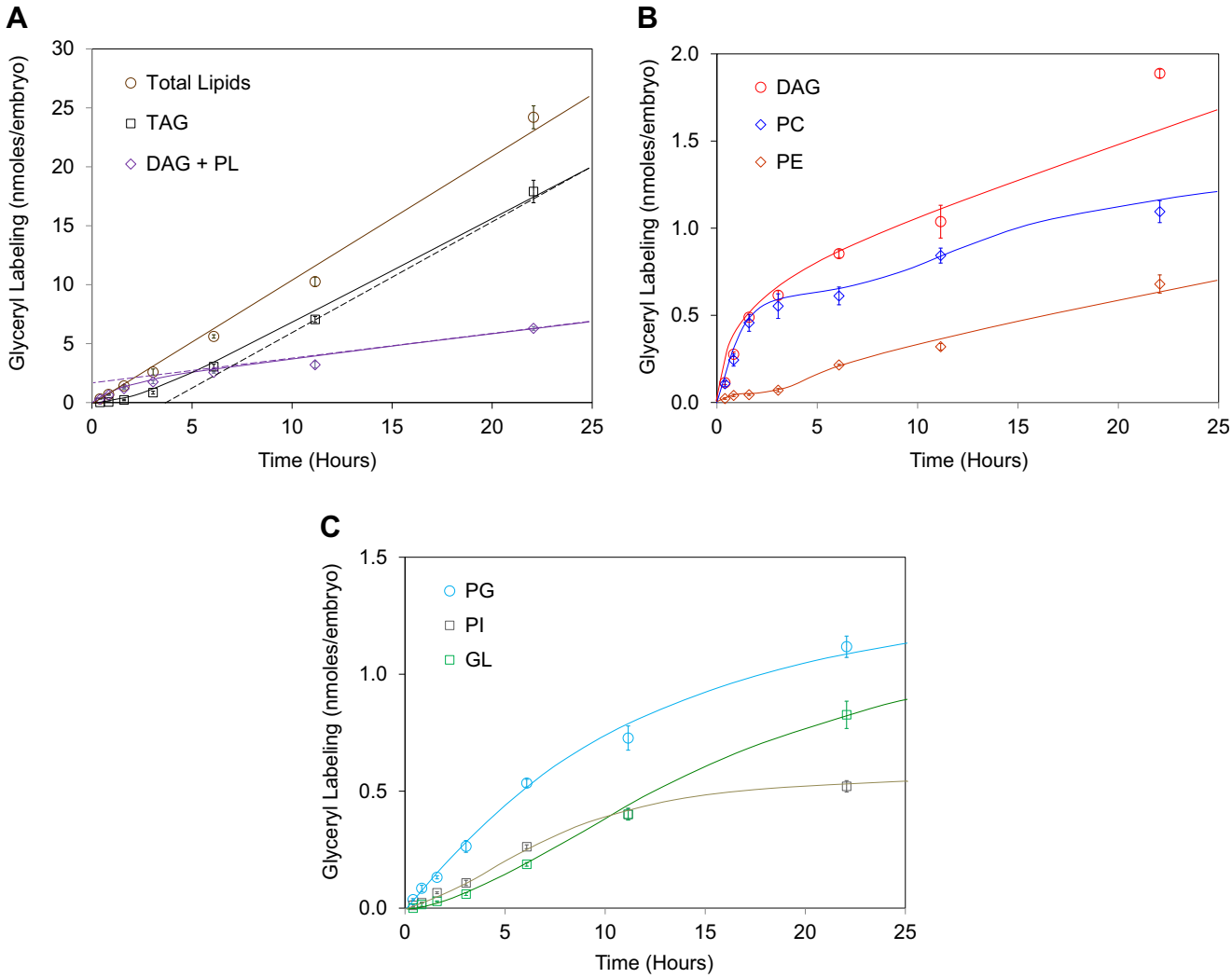

Figure 3. Glyceryl labeling of lipid classes over a culture period of 24 h. *A–C*, assays were run at 2 mM total glycerol (tracer amount of [$^{14}C_3$]glycerol with the remainder as [$^{13}C_3$]glycerol) for up to a period of 22 h. Glyceryl labeling reports the sum of ^{14}C plus ^{13}C labeling and was estimated using the ^{13}C isotopomer calculation protocol. *Curves* are fitted to arbitrary functions, *dashed lines* in panel *A* are fitted to *straight lines* to show the early approach to linear rates. Error bars denote SD (n = 3). Expansions of the early time points are provided in Figure S6.

limited number of data points in the latter part of the Figure 3 time course where steady state kinetics are established. Nevertheless, TAG and DAG + PL accumulations are estimated at ∼0.87 and ∼0.21 nmol/h/embryo, respectively (Fig. 3*A*, *dotted lines*). Combined, they produce an overall rate of ∼1.08 nmol/h/embryo, which is close to the fitted rate = 1.06 nmol/h/embryo for total lipids. The TAG steady state synthesis rate is ∼85% of the total rate of glyceryl incorporation. The *x*-axis intercept from TAG accumulation is ∼2.5 h, the *y*-axis intercept is −2.2 nmol/embryo. This intercept predicts the intermediate pool size at ∼2.6 nmol/embryo. The *y*-axis intercept from DAG + PL accumulation is +1.8 nmol. This allows an independent prediction of the intermediate pool size at ∼2.2 nmol/embryo.

The glyceryl labeling kinetics for individual lipid classes within the DAG + PL intermediate pool are shown in Figure 3, *B* and *C*. Estimates for initial rates of glyceryl labeling over the first hour (nmol/embryo/h) were DAG = 0.33, PC = 0.29, PG = 0.10, PE = 0.05, and PI = 0.03, with GL ≤ 0.02 and TAG = 0.06, to give a cumulative rate = 0.88 nmol/embryo/h for these lipid classes. Thus, 0.18 nmol/h/embryo remains unaccounted for. The nonzero initial TAG labeling rate becomes an important point and is discussed later. DAG and PC contributed the majority of initial rates of *de novo* glycerolipid synthesis, at 31% and 27%, respectively. This observation is consistent across many seed studies, including for linseed (30), Arabidopsis (36), and soybean (10). DAG, PG, and PI showed the expected kinetic behavior, with smooth curves progressing into a steady state linear rate of product accumulation. GL showed a distinct sigmoidal accumulation. Based on a previous lipid analysis of maturing Camelina embryos (23), perhaps 15 to 20% of the GL are prokaryotic in origin (monogalactosyldiacylglycerol containing C16:3 fatty acid). Thus, the bulk of GL will be labeled *via* the cytosolic lipid synthesis pathway before import into the chloroplast, causing sigmoidal labeling kinetics. The most surprising

kinetic behavior was the apparent inverse modulation in the accumulations of labeled PC and PE over 2 to 10 h period (Fig. 3*B*). This requires further investigation.

[$^{13}C_3$glyceryl] lipid class analysis provides estimates of active pool sizes

Figure 4 shows the weighted average mole fraction for [$^{13}C_3$*glyceryl*] over time for TAG, DAG, and PC. The mole fractions for the individual C_n molecular species are reported in Figure S7. In particular, the mole fraction of [$^{13}C_3$*glyceryl*] species in individual C_n TAGs fell in a narrow range (Fig. S7) at each time point and increased in concert over time. This was expected as the total TAG C_n distribution does not change much over time (Table S1). In Figure 4*A*, which is part of the long-term kinetic experiment shown in Figure 2, DAG and PC labeling reached a quasi-linear region by the first time point at 8 h. This initial rapid increase in labeling confirmed their status as intermediates in TAG biogenesis. Extrapolating the slowly increasing rate back to zero time gives intersects of approximately 0.28 and 0.27 mol% for PC and DAG, respectively. These intercepts report labeled active pool sizes for *de novo* acylglycerolipid synthesis. The graphs in Figure 4*B*, which derive from the medium-term kinetic experiment shown in Figure 3, confirm the intercepts derived in Figure 4*A* as approximately 0.30 and 0.28 mol% for PC and DAG, respectively. Furthermore, they show that during the initial active pool filling over the first 1.5 h, the mole fractions of DAG and PC track each other very closely. The similar ^{13}C mole fractions in DAG and PC suggest that in the inactive pool there is substantial DAG, at a DAG to PC ratio found in the active pool.

The curves shown in Figure 4, and particularly Figure 4*A*, require further discussion, with respect to both intermediate lipids DAG and PC, and to TAG end product. In the simplest situation, exogenous label reaches mole fraction A and endogenous metabolites contribute mole fraction B to the active intermediate pool, with the mole fraction not part of the active pool at a constant value C, such that A + B + C = 1. Then, once steady state is reached, the [$^{13}C_3$*glyceryl*] mole fraction will have a constant value. However, beyond the active pool filling period (Fig. 4*B*), the underlying factors determining B and C increasingly change with time, even as [$^{13}C_3$*glyceryl*] incorporation into lipids per embryo remains constant (Figs. 2*A* and 3*A*). There are two key changes. First, intermediate DAG and PC accumulate as end product (whether part of the active pool or not) and thus cause the quasi-linear increase in [$^{13}C_3$*glyceryl*] mole fraction over 8 to 30 h. For this to be observable, mole fraction C must be substantial. In addition to the continuous net accumulation of new DAG and PC per embryo, it is also possible that they slowly displace endogenous PC and DAG, also decreasing the [$^{12}C_3$*glyceryl*] mole fraction C. Thus, in order to match the [$^{13}C_3$*glyceryl*] mole fractions with the parameters shown in Table 1, it is necessary to extrapolate the values back to t = 0 h.

Second, in order to interpret these curves, it is important to recall that over a prolonged assay (up to 6 days), the rate of [$^{13}C_3$]*glyceryl* incorporation per embryo remained constant but that an increase in [$^{12}C_3$]*glyceryl* incorporation over time was also inferred because the total TAG accumulation accelerated (24). This phenomenon was confirmed in this study. Several simple simulations were tested to reproduce the time-dependent increase in the weighted average mole fraction for TAG containing [$^{13}C_3$*glyceryl*] in Figure 4*A*. Three simulations are compared with the experimental average values in Figure 5. Details of the simulations are provided in Figure S8. Simulations that do not allow for a change in the [$^{13}C_3$/$^{12}C_3$*glyceryl*] TAG synthesis ratio cannot provide a close match to the experimental mole fraction curve. However, as shown by simulation 3 as time proceeds, [$^{13}C_3$*glyceryl*]TAG synthesis must be increasingly diluted with the synthesis of [$^{12}C_3$*glyceryl*]TAG. That is, unlabeled carbohydrate supplies an increasing fraction of G3P synthesis to sustain higher rates of TAG synthesis. Simulation 3 suggests

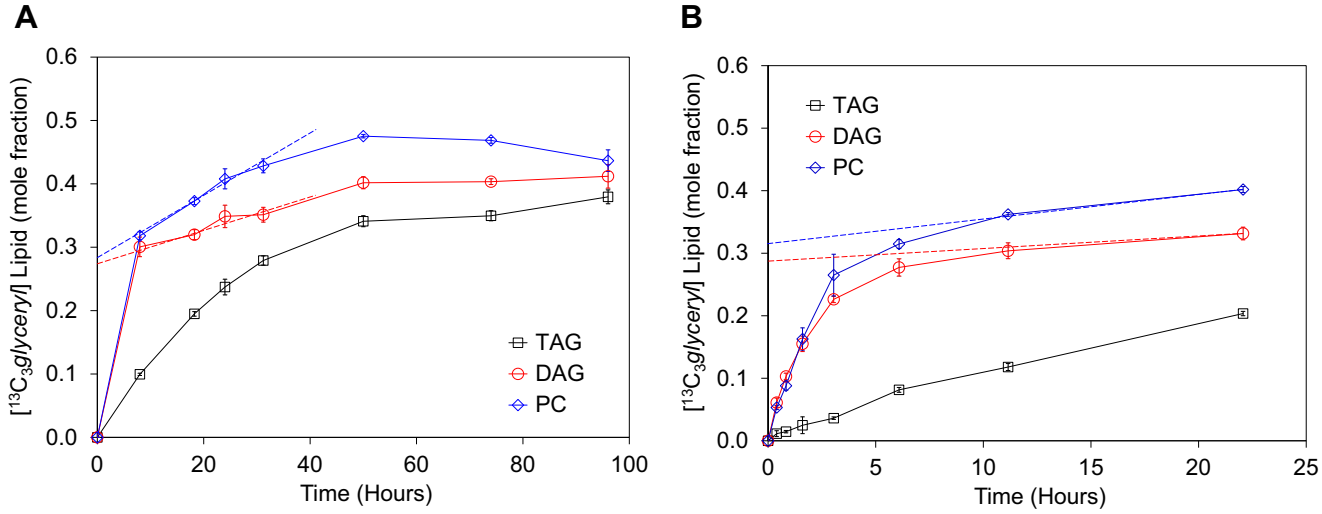

Figure 4. Kinetics of specific activity changes for [$^{13}C_3$*glyceryl*] in major lipid classes. *A*, mole fractions of $^{13}C_3$ glyceryl labeled in total TAG, DAG, and PC, for the long-term time course (shown in Fig. 2). *B*, as in *A*, but for the medium-term time course (shown in Fig. 3). *Dashed lines* show extension of increasing quasi-linear region back to t = 0. Error bars denote ±SD (n = 3). DAG, diacylglycerol; PC, phosphatidylcholine; TAG, triacylglycerol.

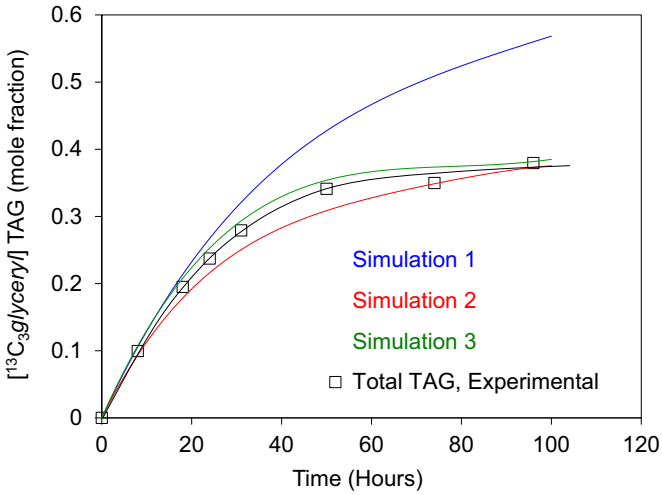

Figure 5. Simulation of TAG [$^{13}C_3$*glyceryl*]-specific activity during a culture period of 4 days. TAG average specific activity values are taken from Figure 4*A*. The simulations are described in detail in Figure S5. Simulations 1 and 2 maintain a constant [$^{13}C_3$/$^{12}C_3$*glyceryl*] ratio for TAG synthesis over the assay period, even as the rate of [$^{13}C_3$*glyceryl*]TAG accumulation remains constant. In simulation 1, where the ratio is set at 10:2, such that it closely matches the experimental mole fraction change for the first two time points, the simulation greatly overestimates the increase in specific activity as the culture progresses. Also, the total TAG present in the embryos at the end of the assay is 32% too low. In simulation 2, the ratio is changed to 10:11, which provides the correct amount of TAG at the end of the assay, but the curve fit with experiment is inexact. Simulation 3 allows incremental steps increasing the ratio with time, rising from 10:2 to 10:14, allowing a close fit for both end-point TAG accumulation and the change in mole fraction over time. TAG, triacylglycerol.

that early on in the time course, [$^{13}C_3$*glyceryl*] substrate is only modestly diluted by [$^{12}C_3$*glyceryl*] substrate, of the order of 20%, but it allows the rate of total TAG accumulation to double over 4 days.

Biosynthetic (M + 2), (M + 3), and (M + 5) labeling calculations based on a single system appear invalid

The ^{13}C isotopomer multiplets were deconvoluted into their major biosynthetic components, (M + 2), (M + 3), and (M + 5). A full list of labeling results from [$^{13}C_3$]glycerol (^{13}C mole fraction, isotopomer distributions) across all 10 TAG, DAG, and PC molecular species (Fig. 1) for both the intermediate-term and steady state time courses is provided in Table S2. If glyceryl and acyl labeling from exogenous glycerol is considered in terms of a single biochemical system, arithmetic analysis of the molar (M + 2), (M + 3), and (M + 5) biosynthetic ratios can be used to predict total biosynthetic products, including unlabeled contributions. Table 2, part A shows the equations for this prediction. They use two variables, namely the ratio of the rate of accumulation of [$^{13}C_3$*glyceryl*] to [$^{12}C_3$*glyceryl*] in total lipids (1: x mol), and the ratio of the rate of accumulation of [$^{13}C_3$*glyceryl*] to [$^{13}C_2$*acyl*] in total lipids (1: y mol). Experimental estimates (x = 0.3 mol and y = 0.2 mol), taken from Figures S4*B* and 5, respectively, are then used as inputs to generate isotopomer distributions. More generally, simulations could be run where x and y varied over the course of the assay.

It is important to assess the validity of this approach. An example is shown in Table 2, part *B*. At the earliest time points, DAG and PC are codominant-labeled products, whereas TAG labeling lags (Fig. 3). Consideration of the (M + 2), (M + 3), and (M + 5) distributions in DAG and PC at the earliest time points (Table 2, part B) invalidates the idea of describing glyceryl and acyl labeling as derived from a single system using exogenous glycerol uniformly across the embryo. The contribution from [$^{12}C_3$*glyceryl*] lipid relative to [$^{13}C_3$*glyceryl*] lipid can be calculated for these data according to the single system hypothesis, that is (M + 2)/(M + 5) = $x \sim$ 0.3. However, the measured (M + 2)/(M + 5) values are >>1 for DAG and >1 for PC, greatly in excess of the single system prediction. They would predict net synthesis rates for each of these intermediates greatly in excess of the observed net synthesis rate for total lipids. This analysis is the most striking among several examples of large inconsistencies that arise when the isotopomer data are interpreted on the basis of a single biosynthetic system. Thus, it is necessary to postulate that lipid [$^{13}C_2$*acyl*] labeling is largely disconnected from

Table 2
DAG and PC (M + 2), (M + 3), and (M + 5) molar distributions at early time points

A: Formulae for prediction based on a single biosynthetic system

For 1.0 mol [$^{13}C_3$*glyceryl*] incorporation plus x *mole of* [$^{12}C_3$glyceryl] *incorporation, plus* y *mol of* [$^{13}C_2$acyl] *incorporation*

Formulae	Calculated values For x = 0.3 mol, y = 0.2 mol	Observed[a]
(M + 0) = $x - (x.y/(1 + x))$ moles	0.2538 mol	
(M + 2) = $x.y/(1 + x)$) moles	0.0462 mol	4.4 mol%
(M + 3) = $(1 - y/(1 + x))$ moles	0.8462 mol	80.9 mol%
(M + 5) = $y/(1 + x)$ moles	0.1538 mol	14.7 mol%

B: Experimental (M + n) distributions at early time points

	Time (h)	(M + 2)	(M + 3)	(M + 5)	(M + 2)/(M + 5)
DAG	0.4	75 ± 2%	24 ± 2%	1 ± 1%	75
	0.83	47 ± 8%	52 ± 8%	1 ± 1%	47
	1.58	28 ± 2%	71 ± 1%	1 ± 1%	28
PC					
	0.4	22 ± 7%	71 ± 8%	7 ± 3%	3.1
	0.83	4 ± 2%	94 ± 4%	2 ± 2%	2.0
	1.58	7 ± 5%	87 ± 4%	6 ± 2%	1.2

(M + 2), (M + 3), and (M + 5) molar distributions are weighted averages across C34–C38 acyl carbon DAG or PC species, with C36 being the major species.
[a] (M + 0) represents the unlabeled biosynthetic contribution over the assay period. It cannot be observed directly because signal also includes unlabeled lipid present prior to the assay. However, both x and y can be calculated from measured isotopomer mole % distributions so that an estimate can be made of (M + 0) to the flux analysis.

[$^{13}C_3$*glyceryl*] labeling, and therefore, the existence of more than one lipid biosynthesis system in the embryos.

Lipid labeling from glycerol provides evidence for distinct TAG synthesis systems

The previous section showed that treating glyceryl and acyl labeling of lipids from exogenous glycerol as a unified whole is incompatible with the labeling data. Plotting the medium-term time course datasets for TAG, DAG, and PC independently for (M + 2), (M + 3), and (M + 5) biosynthetic products (Fig. 6) resolves the problem. In the medium-term experiment (Fig. 6*A*), the steady state rate of incorporation into [$^{13}C_2$*acyl*] lipids was 0.231 nmol/h/embryo, representing 17.6 mol% of total glycerol incorporation. [$^{13}C_3$*glyceryl*] and [$^{13}C_2$*acyl*] labeling are shown in Figure 6*A*. This contrasts with data for the long-term kinetic experiment (Fig. S4*B*), where the steady state rate of incorporation of glycerol into [$^{13}C_2$*acyl*] lipids was 0.397 nmol/h/embryo, representing 24.6 mol% of glycerol incorporation into total lipids.

Figure 6*B* shows the time dependence for TAG isotopomer labeling. The dominant TAG synthesis is provided by (M + 3) species, with the expected lag phase for precursor pool filling and zero initial rate. For a simple single TAG synthesis system *via* DGAT or PDAT, the (M + 5) labeling would be expected to have a similarly shaped curve but at a lower concentration. It should also have no crossover with the (M + 3) curve. The (M + 2) contribution would be expected to level off beyond the (M + 3) lag phase. However, both (M + 2) and (M + 5) appear to show approximately linear rates of accumulation over the time course, at rates of approximately 0.18 and 0.11 nmol/h/embryo, respectively, and with intersections close to the origin. Thus, they follow similar kinetics that are independent of the (M + 3) TAG synthesis rate. The steady state rate for (M + 3) TAG synthesis (rate over the last two time points) is estimated as 0.86 nmol/h/embryo, with an intersection of ∼3.5 h on the *x*-axis. Its effective precursor pool size is therefore ∼3 nmol/embryo. The TAG synthesis system showing (M + 3) labeling thus contributes ∼75% of the total TAG synthesis flux, whereas the TAG synthesizing system(s) resulting in (M + 2)

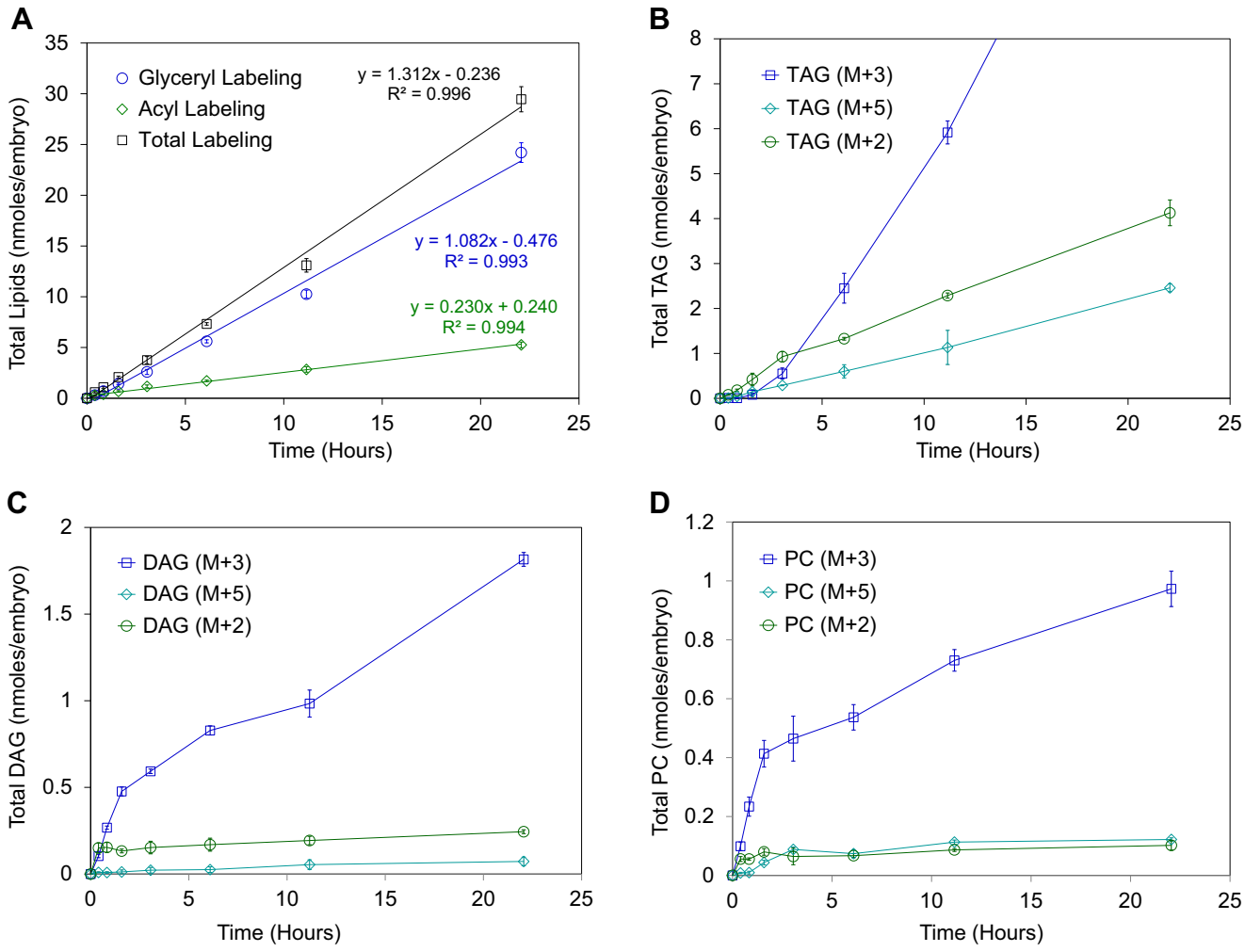

Figure 6. Acyl and glyceryl labeling from [$^{13}C_3$]glycerol and accumulation of individual (M + 2), (M + 3), and (M + 5) isotopomer products for TAG, DAG, and PC. See the legend to Figure 3 for further experimental details. *A*, accumulation of total ^{13}C units and [$^{13}C_3$]glyceryl and [$^{13}C_2$]acyl unit components in total lipids, with best straight line fits. *B–D*, biosynthetic isotopomer distributions in total TAG, DAG, and PC, respectively. Error bars denote SD (n = 3). DAG, diacylglycerol; PC, phosphatidylcholine; TAG, triacylglycerol.

and (M + 5) labeling comprising a combined rate of 0.18 + 0.11 = 0.29 nmol/h/embryo contributes the other ~25% of embryo total TAG synthesis.

Figure 6, *C* and *D* shows the time dependence for DAG and PC isotopomer accumulation, respectively. Again (M + 3) species dominate, providing active intermediate pool filling for TAG synthesis followed by a slow net accumulation phase. The level of (M + 2) DAG, however, peaks at the earliest time point (0.4 h) and then stays approximately constant at ~0.15 nmol/embryo. Thus, it could provide a precursor pool for (M + 2) TAG synthesis. (M + 2) PC accumulation appears similar to (M + 2) DAG, though the steady state level is less at ~0.07 to 0.10 nmol/embryo. (M + 5) DAG appears to steadily accumulate at a very low rate of ~0.03 nmol/h/embryo, whereas (M + 5) PC only reaches its maximum at 3 h, at ~0.10 nmol/embryo.

It is possible to make a rough estimate of relative rates for the metabolism that produces (M + 3) TAG (system A) and of (M + 2) plus (M + 5) TAG (system B). Writing G*A for (M + 3), GA* for (M + 2), G*A* for (M + 5), and GA for (M + 0), then to a first approximation, we have system A comprising 9 mol G*A and system B comprising 2 mol GA* + 1 mol G*A*, with 1 mol GA that might be assigned to either A or B: in total, the embryos are labeled with 10 mol G*, 3 mol G, and 3 mol A*. Previously, we noted that in the long-term time course, the molar ratio of glyceryl to acyl was 1 to 0.31. This dropped to 1 to 0.21 in the medium-term time course. Furthermore, it was expected that there be a molar ratio for labeling of [$^{13}C_3$*glyceryl*]lipid to [$^{12}C_3$*glyceryl*]lipid of about 1 to 0.3. Thus, the chance of any given acyl group C2 unit being labeled relative to labeled glyceryl (=100%) falls from 1.2% to 1.2 × (0.21/0.32) × (1.0/1.3) = 0.59%. The TAG (M + 2n) isotopomer content for this level of acetyl labeling can be read directly from Figure S1. Separating out G* from (G* + A*) labeling implies that there must be increased concentration of A* labeling, as given by Figure S1. This means that (M + 2n) must increase. According to the numerical approximation just presented, the acetyl unit labeling would increase by 3.1-fold, that is from a 0.59% to a 1.9% chance. This still produces the major acyl-labeled TAG as (M + 2) not (M + 4). This analysis suggests that about 23 to 31% of embryo TAG synthesis could be *via* "system B" as estimated previously.

TAG isotopomer distributions vary with tissue and solvent extractability

The observation that (M + 3) isotopomers of lipids labeled from glycerol showed highly distinctive kinetics when compared with (M + 2) and (M + 5) isotopomers (Fig. 6) was unexpected. This differentiation must represent separate kinetic systems and calls for an explanation. Discounting separate systems operating together in the same cell, which seems unlikely, that leaves explanations based on tissue and cell types and possible differential development of such tissue layers and/or cells. Two relatively straightforward experiments were conducted to probe such possibilities. They did not require sophisticated imaging methods to distinguish isotopomer profiles *in situ* or laser dissection methods of isolating cell types. The experiments involved incubation of intact embryos with [$^{13}C_3$]glycerol and either dissection of the embryos into parts prior to lipid extraction or tracking the kinetics of lipid extraction from intact embryos. In these experiments, a 4 h labeling period was chosen so as to combine sufficiently high total ^{13}C incorporation while retaining a ^{13}C distribution that was not dominated by a single isotopomer, such that the S/N for each isotopomer in different tissues or extract fractions was adequate for quantitation.

For embryo dissection into inner cotyledon, outer cotyledon, and axis after assay, dissections were facilitated by the fact that with increased time in culture, the inner and outer cotyledons became less appressed and rotated at different rates to the open position (Fig. S9). The molar distribution of TAG acyl carbon number molecular species in dissected embryo tissues (Fig. 7) showed that the TAG compositions of inner and outer cotyledons were very similar, with only a very slight enhancement of C56 and C58 TAGs in the outer and larger cotyledon. However, the axis had substantially less C56 and C58 TAGs, with concomitant increases of C50–C54 TAGs. These TAG distributions are consistent with the FAME compositions reported in Figure S10 and Table S3. The (M + 2), (M + 3), and (M + 5) molar distributions in total TAG and individual acyl carbon number TAG molecular species are reported in Table 3 for inner cotyledons, outer cotyledons, axis, and whole embryos (control). The summation for total TAG distribution in the dissected parts agrees with that for the whole embryo, suggesting that the dissection process had no significant effect on the distributions. The isotopomer distributions summed for total TAG for each of the parts are very similar for the axis and outer cotyledon, but the inner cotyledon deviates slightly in that the (M + 3) is slightly higher and the (M + 2) is slightly lower. However, despite this small

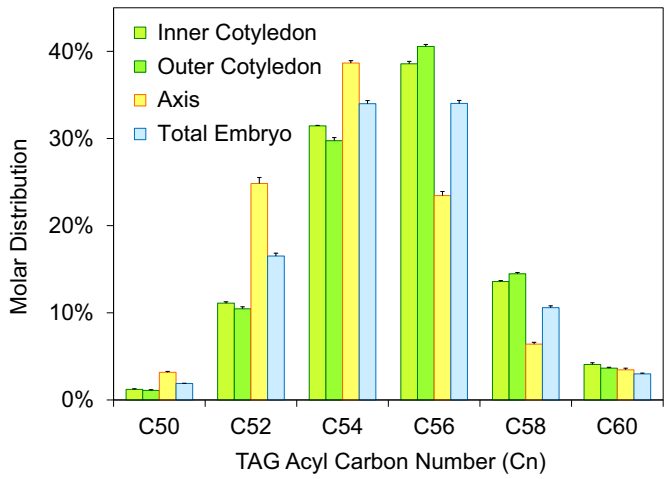

Figure 7. Molar distribution of TAG acyl carbon number molecular species in dissected embryo tissues. After assay for 4 h with [$^{13}C_3$]glycerol, embryos were dissected into axis, inner cotyledon, and outer cotyledon prior to assay quenching and lipid extraction, with a control group for intact embryos. Assays were run in quadruplicate with 24 embryos/assay. ESI–MS analysis was conducted on hydrogenated TAGs. The molar distribution of TAG acyl carbon number molecular species is shown. Error bars denote ±SD (n = 4). ESI, electrospray ionization; TAG, triacylglycerol.

Table 3
Total TAG, TAG acyl carbon number molecular species, and (M + 2), (M + 3), and (M + 5) molar distributions, in inner cotyledons, outer cotyledons, and axis in a short-term assay with [$^{13}C_3$]glycerol

	TAG (mole %)[a]						
	C50-TAG	C52-TAG	C54-TAG	C56-TAG	C58-TAG	C60-TAG	Total TAG[b]
Inner cotyledon							
Mass[c]	1.2 ± 0.1	11.1 ± 0.2	31.5 ± 0.1	38.6 ± 0.3	13.6 ± 0.1	4.1 ± 0.2	23.2 ± 0.1
(M + 2)		28.5 ± 4.5	30 ± 2	36.5 ± 2.5	63.5 ± 4		42.5 ± 0.5
(M + 3)		61 ± 9	63.5 ± 2.5	55 ± 2	26.0 ± 4.5		49 ± 1.5
(M + 5)		10.5 ± 5.5	6.5 ± 1.5	8.5 ± 0.5	10.5 ± 1.5		8.5 ± 1
Outer cotyledon							
Mass[c]	1.1 ± 0.1	10.5 ± 0.2	29.8 ± 0.4	40.6 ± 0.2	14.5 ± 0.2	3.6 ± 0.1	40.4 ± 2.7
(M + 2)		27 ± 5	28 ± 6	55 ± 6	67 ± 11		48.5 ± 6.5
(M + 3)		64 ± 3	64.5 ± 4	37.5 ± 6	26 ± 10		44 ± 6
(M + 5)		9 ± 3	7.5 ± 3.5	7.5 ± 1.5	7 ± 1		7.5 ± 1.5
Axis							
Mass[c]	3.2 ± 0.1	24.8 ± 0.7	38.7 ± 0.3	23.5 ± 0.5	6.4 ± 0.2	3.5 ± 0.2	38.7 ± 2.7
(M + 2)		33 ± 6.5	40 ± 10	55.5 ± 6.5	63 ± 4		48.5 ± 3.5
(M + 3)		62 ± 6	55 ± 11	32.5 ± 4.5	16 ± 9		41 ± 1.5
(M + 5)		5 ± 2.5	5 ± 4	12 ± 4.5	21 ± 7		10.5 ± 3
Summed dissections							
Mass							100
(M + 2)							45.5 ± 2
(M + 3)							44.5 ± 1.5
(M + 5)							10 ± 2
Whole embryo							
Mass[c]	1.9 ± 0	16.5 ± 0.3	34.0 ± 0.4	34.0 ± 0.3	10.6 ± 0.2	3.0 ± 0.1	100
(M + 2)		29 ± 10	34 ± 3	48 ± 7	54.5 ± 5		42.5 ± 2.5
(M + 3)		65.5 ± 10	60.5 ± 3.5	45 ± 10	36 ± 7		50.5 ± 4.5
(M + 5)		5.5 ± 2.5	5.5 ± 4.5	7 ± 4	9.5 ± 4		7 ± 3

[a] Error bars denote ±SD (n = 4).
[b] Totals for TAG mass distribution are summed as mole % over dissected tissues, whereas totals for TAG^{13}C isotopomer profiles are summed as mole % over all Cn TAG species over (M + 2) + (M + 3) + (M + 5) isotopomers. "Total TAG" summed over dissected tissues.
[c] Mass Cn TAG distribution is also reported in Figure 7.

difference, it is clear that the larger flux system (M + 3 isotopomer) and lower flux system (M + 2 and M + 5 isotopomers) extend across all three embryo parts without major changes in distribution. Also noteworthy, (M + 2) isotopomer is enriched in C56-TAG and even more so in C58-TAG, a pattern seen across all three tissues. The (M + 5) isotopomer is largely independent of TAG acyl carbon number for both inner and outer cotyledons. However, in the axis, (M + 5) is more pronounced in C56-TAG and most pronounced in C58-TAG.

Sequential batch solvent extraction of embryos produced small but possibly significant changes in molar distribution of TAG acyl carbon number molecular species with extraction time. These are reported and briefly discussed in Figure S11 and likely point to modest differential extraction of different Cn species. The differential extraction rates of (M + 2), (M + 3), and (M + 5) TAG isotopomers are shown in Figure 8. Figure 8*A* shows that the amounts of TAG mass extracted sequentially from intact embryos are 3%, 10%, and 27%, respectively, with 60% remaining in the embryo and recovered by final homogenization and extraction. With the successive extractions, (M + 2) isotopomer content falls significantly, whereas (M + 3) isotopomer content increases. (M + 5) isotopomer content shows a slight decline. Figure 8*C*, derived from absolute values shown in Figure 8*B*, shows the relative recovery for each sequential extraction, total sum = 100%, for each isotopomer for each acyl carbon number TAG molecular species. The relevant comparison is to the total TAG extraction. Extraction of (M + 3) isotopomers, which are the dominant product at steady state biosynthesis, track total TAGs closely, a self-fulfilling result. (M + 3) C56-TAGs and C58-TAGs are extracted slightly more slowly than (M + 3) C52-TAGs and C54-TAGs. However, both (M + 2) and (M + 5) TAG isotopomers are extracted relatively more efficiently at earlier time points. Plotting the data as mole fractions in total TAG (Fig. 8*B*) highlights the fact that the majority of the (M + 2) and (M + 5) species are found in the C56 and C58 TAGs. Since C58 TAG is only the fourth most abundant molecular species, with a molar abundance of half that of C56 TAG, the (M + 2) labeling of C58 TAG has the highest enrichment.

Discussion

If an embryo can be considered as a single homogeneous kinetic system, this makes the task of translating kinetic datasets into a metabolic flux map considerably easier than if interpretation requires additional complexity such as distinctive cell types and/or organelles. Multiple pools postulated in order to explain flux analysis results must have biological underpinnings. Previous studies with cultured and mid-maturation Camelina embryos suggested that lipid labeling from acetate and glycerol substrates might be interpreted in terms of whole system labeling (24). At kinetically saturating levels, exogenous acetate labeled about 5 mol% of the C2 flux to fatty acids, in a manner consistent with a relatively uniform utilization across the embryo. Saturating exogenous glycerol provided about 70 to 80 mol% of the glyceryl groups for acyl lipid biosynthesis. Thus, it was considered probable that glycerol labeling would be consistent across the embryo. However, interpretation of labeling results based on a single

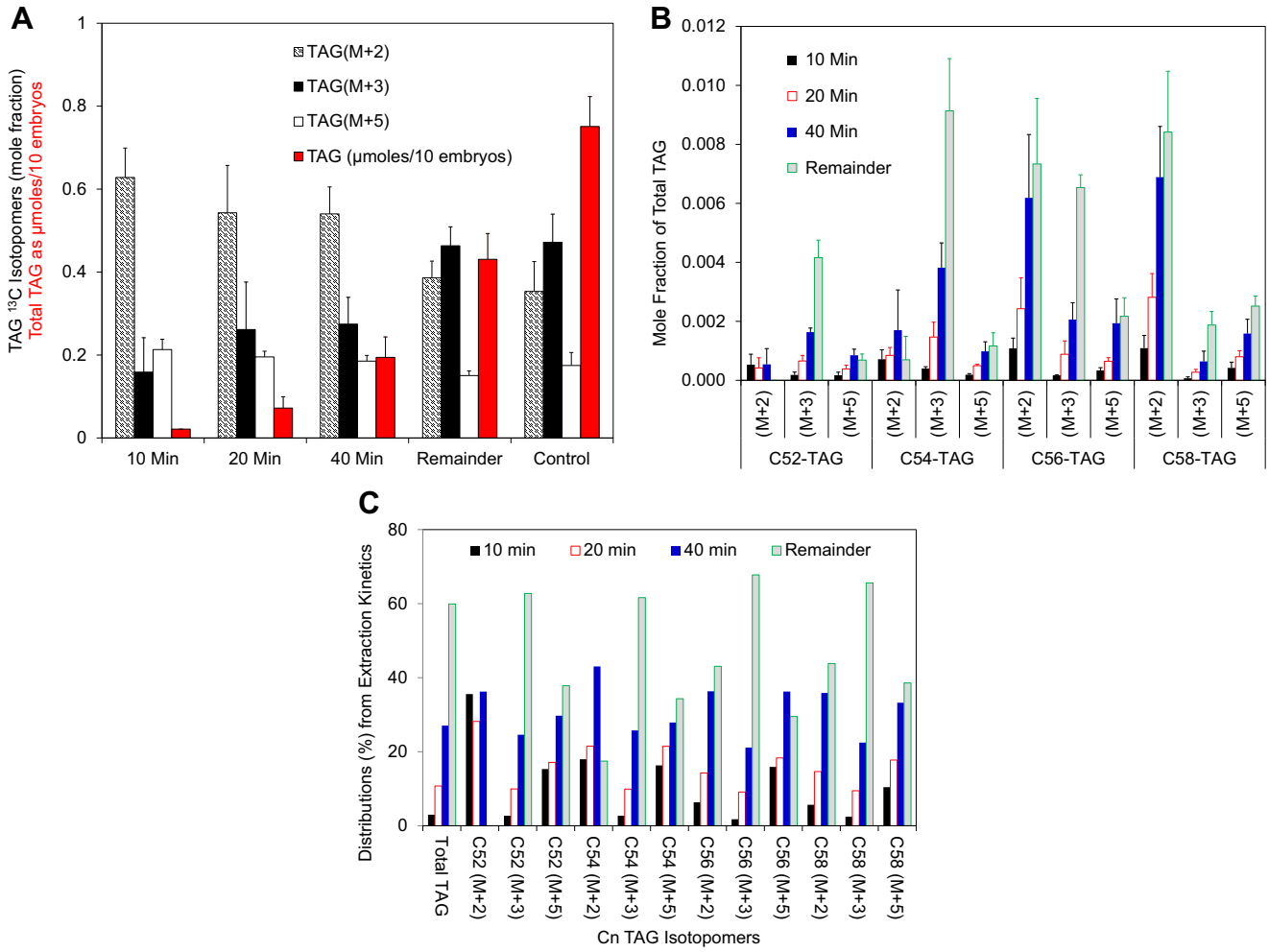

Figure 8. Differential extraction rates of (M + 2), (M + 3), and (M + 5) TAG isotopomers in a short-term embryo assay with [$^{13}C_3$]glycerol. After assay for 4 h with [$^{13}C_3$]glycerol, lipids were extracted from intact embryos for 10, 20, and 40 min sequential periods using chloroform–methanol. The embryos were then homogenized and extracted to recover the remaining lipid. A control, where intact embryos were immediately homogenized and lipids extracted, was included. Assays were run in quadruplicate with 36 embryos each. Isotopomer analysis was conducted on hydrogenated TAGs. *A*, molar isotopomer distributions for total TAG (the mass of total TAG extracted is also shown, in *red*, with identical numerical units). *B*, extraction profile for each isotopomer for each TAG acyl carbon number molecular species, as a mole fraction of total TAG. *C*, averaged absolute determinations from (*B*) utilized to present the percent extractability for each isotopomer for each TAG acyl carbon number molecular species across the extraction kinetic sequence. Error bars denote ±SD (n = 4). TAG, triacylglycerol.

kinetic system now appears to be invalid. The kinetic and pool size data presented in the first part of the Results section must be reinterpreted in the context of the multiple systems described subsequently. The assumption that since the mid-maturation embryo is dedicated to storage accumulation, the complete degradation of both acyl and glyceryl moieties in lipids are negligible was not challenged in this study. Measurements of incorporation into glyceryl and acyl groups are therefore assumed to be both *de novo* biosynthesis and net reaction rates.

Glyceryl labeling kinetics

Glycerol labeling of embryo lipids was linear over an extended culture period (Figs. 6*A* and S4*B*): acyl and glyceryl components of this glycerol labeling were also linear, except over the first hour or two, when the acyl to glyceryl ratio fell. To reiterate, glyceryl labeling is the sum of biosynthetic (M + 3) and (M + 5) isotopomers, that is, [$^{13}C_3$*glyceryl*] plus [$^{13}C_2$*acyl* + $^{13}C_3$*glyceryl*] species respectively; acyl labeling is the sum of biosynthetic (M + 2) and (M + 5) isotopomers, that is, [$^{13}C_2$*acyl*] plus [$^{13}C_2$*acyl* + $^{13}C_3$*glyceryl*] species, respectively. Steady state rates showed that 87 mol% of glyceryl groups from exogenous glycerol were incorporated into TAG, with 0.7 mol% in DAG and 12 mol% in PL (includes 4 mol% as PC). These are consistent with the lipid class molar distributions measured in zygotic embryos at 16 days post anthesis (DPA) (89 mol% TAG, 1.2 mol% DAG, 9.8 mol% PL [4.4 mol% PC], Table 1 and (23)). Comparing [$^{13/14}$C]glyceryl accumulation rate of 1.22 nmol/h/embryo (Fig. 2*A*) with the total glyceryl accumulation rate of 1.54 nmol/h/embryo (*i.e.*, exogenous plus endogenous substrate) showed that exogenous glycerol contributed 79% of total glyceryl used in lipid synthesis early in the assay. This value fell to 40% by day 4 in culture, even as the [$^{13/14}$C]glyceryl accumulation rate stayed constant, because the total glyceryl accumulation rate rose to

3.205 nmol/h/embryo. This rise is consistent with previous studies of Camelina embryos in prolonged culture (23, 24).

Kinetic analyses of the [$^{13/14}C$*glyceryl*] intermediate pool size based on intercepts for TAG accumulation or for the combined DAG + PL fraction gave values of 5.18 and 5.22 nmol/embryo, respectively. Thus, the labeled DAG + PL fraction is the same size as the intermediate pool required for TAG synthesis. This pool size, 5.2 nmol/embryo, and a steady state rate of 1.22 nmol/h/embryo give the half-life for glyceryl-labeled intermediates in the TAG precursor pool as 3.0 h, consistent with TAG labeling kinetics. Thus, the kinetics of lipid assembly in the culture system, as tracked by glyceryl labeling, are self-consistent and represent a fully operational pathway producing the expected composition and rate. They define DAG and PL as key intermediates and give good estimates of the sizes of the intermediate pools. Kinetic flux modeling can proceed based on this foundation. An important observation is that DAG and the individual PL species do not reach a constant level of labeling, indicating a constant size for the active pool, but continually accumulate. Whether this indicates an expanding active intermediate pool or diversion to an "inert" end product pool cannot be ascertained from this experiment (Fig. S5).

The kinetic analysis so far has treated glyceryl labeling as a whole, but data presented in Figure 6 in particular show that [$^{13}C_3$]glycerol incorporation into the TAG glyceryl backbone combines both a dominant kinetic system A, for (M + 3)TAG, and a minor system B, for (M + 5)TAG. (M + 5)TAG accumulation was essentially linear and contributed about 10% of the steady state–labeled glyceryl incorporation. As indicated by simulation (Fig. S5), if the total [$^{13}C_3$]glyceryl rate estimated by the *x*-axis intercept in Figure 2 gives $t_{1/2}$ = 2.95 h, then for (M + 3)TAG, the corresponding value will be $t_{1/2}$ = 2.95 × (1/(1–0.1)) = 3.28 h. As (M + 5)TAG accumulation is already linear at the first time point (24 min), any pool filling for this system gives $t_{1/2} << 0.4$ h. Clearly, the intermediate pool–filling kinetics for glyceryl TAG synthesis is dominated by (M + 3) isotopomers, which show much larger rate and half-life values.

The shorter glyceryl labeling time course (Fig. 3), which showed initial rates and entry into steady state, gave a total lipid synthesis rate estimated at ∼87% of that measured in Figure 2, with intermediate pool size significantly lower at ∼44%. Thus, $t_{1/2}$ for the intermediate pool was ∼1.6 h. Given that the total rate of lipid accumulation increases over embryo culture, one explanation of the quantitative differences between the two time courses may be that embryos were at a slightly earlier stage of development in the experiment shown in Figure 3. As expected, the proportion of the initial rate of glyceryl incorporation was highest for DAG (36%) and PC (30%), with other PLs together constituting about 20% and TAG about 13%. This estimate of the TAG initial rate from Figure 3 will be the system B (M + 5)TAG component. However, the TAG synthesis rate rose to about 83% of the total rate. Comparing the initial glyceryl labeling rates from Figure 3 with the estimates of lipid intermediate pool sizes from Figure 2, the initial rates underestimate (by approximately threefold) the contributions of PE, PG, PI, and GL relative to DAG and PC for TAG synthesis, as predicted by the long-term pool size analysis. Presumably, glyceryl-labeled DAG and PC are converted to these other membrane lipids but become available for TAG synthesis by retroconversion mechanisms. Thus, a rebalancing of phospholipid composition will be required for any comprehensive flux model. This interaction between neutral and membrane lipid biosynthesis requires further elucidation.

Multiple pools of DAG and PC coexist

The idea that multiple lipid pools exist within plant tissues is not novel. A lipid class found in multiple organelles can be considered as a collection of distinct pools. Likewise, running experiments with tissues such as "leaf" or "embryo," which contain a multiplicity of cell types (and cell cycle stages) will combine the kinetic characteristics for each cell type to give an average value. To define individual pools kinetically is more problematic, as the time constant for a process will define what is or is not a pool. Pools may or may not have distinctive molecular species compositions. Clearly, the distinction in lipid acyl compositions between axis and cotyledons of Camelina seeds (Figs. 7 and S8, and (25)) will lead to expectations of metabolic heterogeneity. However, the distinctive system A/B kinetic classification appears largely independent of TAG acyl carbon number and of axis and cotyledon, respectively.

In proposing metabolic networks in order to explain experimental kinetic or isotopomer data, it may be necessary to postulate two or more distinct metabolic pools for individual metabolites. Additional knowledge, such as the localization of the metabolite in different organelles or cell types, will help to identify such modeling inferences. In producing a model to describe lipid biosynthesis in developing soybean embryos, it was necessary to postulate two PC and three DAG pools operating within the cell to explain kinetic and compositional data (10). In Camelina embryos, [$^{13}C_3$*glyceryl*] labeling of DAG and PC, the principal intermediates in the synthesis of TAG, rose to initial maximum levels of 0.28 and 0.29 mol% of total embryo amounts, respectively (Fig. 4). However, it is crucial to know what the "endogenous" contributions to the active lipid pools are in order to assess if there are multiple lipid pools present. The term "endogenous" is used here to mean glyceryl groups derived from unlabeled sugars present in the culture during assay. Previously, it was shown that for cultured Camelina embryos at saturating glycerol concentrations, the glyceryl incorporation rates were linear over many days and that over the first few days exogenous glycerol provided the majority of the glyceryl groups for lipid biosynthesis (24). Early in the assay, exogenous glycerol contributed 76.5% of total glyceryl used in net lipid biosynthesis. That is, for every mole of [$^{13}C_3$*glyceryl*], 0.31 mol of [$^{12}C_3$*glyceryl*] was also utilized. Thus, simple addition of ^{13}C and ^{12}C components would lead to the total active pool estimate ≈37 mol%. This is an overestimate because it is necessary to parse out the complex effects of systems A and B. System B has a lower flux and a much lower intermediate pool size, plus a different utilization of exogenous glycerol. Thus

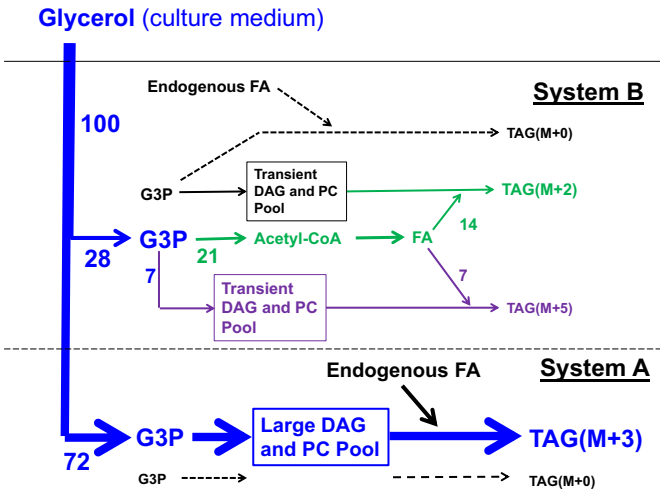

Figure 9. Schematic for utilization of exogenous glycerol in lipid synthesis by midmaturation of *Camelina sativa* embryos in culture. [$^{13}C_3$] Glycerol uptake and incorporation into glyceryl-labeled lipids (M + 3) is shown in *blue*; utilization to provide fatty acids and (M + 2) acyl-labeled lipids is shown in *green*; whereas the mixed acyl plus glyceryl labeling (M + 5) is shown in *purple*. The figures are molar fluxes of [$^{13}C_3$]glycerol utilized relative to 100 mol of substrate uptake; the thicknesses of the *arrows* approximate to the fluxes. *Black lines* represent metabolism fueled by unlabeled metabolites (derived from sugars). The contribution of unlabeled glyceryl groups to lipid synthesis is small, and the unlabeled TAG product formed during the assay is even smaller. This TAG (M + 0) product has been arbitrarily distributed equally between system A and system B. Based on the fact that the net TAG synthesis flux for system A is about 75% of the total, and that the intermediate pool half-lives for A and B are about 180 and <20 min, respectively, the intermediate lipid pool for system A at least 36-fold greater than for system B. TAG, triacylglycerol.

calculated, ∼0.1 mol of [$^{12}C_3$*glyceryl*] per mol of [$^{13}C_3$*glyceryl*] represents an upper correction limit, giving the active intermediate pool sizes for TAG synthesis of ∼31 mol%.

If the active pool sizes for DAG and PC are ∼31 mol% of embryo total amounts, the corollary is that ∼69 mol% of these lipids are not involved in *de novo* glycerolipid synthesis: that is, there must be at least two pools for each lipid. The fact that ∼69 mol% of these lipids are not involved in *de novo* glyceryl metabolism does not imply that they are inactive in acyl editing cycles or that they do not have their own and independent head group reactions. It is also pertinent to note that the pool filling process we have been measuring is of the order of 3 to 4 h. Metabolic process may still be occurring between these pools but with much longer time constants. However, the important point is that quantitative evidence for distinct metabolic pools in two important lipid classes in plant cells has been obtained, independent of any network model.

Evidence of and possible explanations for two glyceryl labeling systems

The idea that seeds may contain multiple lipid synthesis systems was first encountered from *in vivo* acetate-labeling assays with developing nasturtium (*Tropaeolum majus*) seeds (38). For Camelina, distinctly different kinetics for TAG (M + 3) isotopomer synthesis *versus* TAG (M + 2) and (M + 5) isotopomer synthesis were observed (Fig. 6*B*). This finding alone requires that there be two distinct systems for TAG synthesis in embryos, as shown in Figure 9. TAG (M + 3) isotopomer synthesis ("system A") is the major system, representing about 75 to 80% of the total TAG biosynthetic flux. Furthermore, kinetics of DAG and PC (M + 3) isotopomer synthesis showed them to be the intermediates for system A TAG synthesis. This intermediate pool filling process takes several hours. By contrast, TAG (M + 2) and (M + 5) isotopomer synthesis rates are already essentially linear by the first time point (20 min). Together, they are defined as "system B". Because the (M + 2) isotopomer pools of DAG and PC are already filled by the first time point and the DAG and PC (M + 5) isotopomer levels are too low to accurately measure early in the time course and are not synchronous with TAG accumulation, it is not possible to postulate clearly defined relationships between linear TAG (M + 2) and (M + 5) isotopomer syntheses and their putative intermediate pools, other than to say they are consistently small. Thus, system B could be more heterogeneous and complex than implied by the "system B" label.

In addition to distinctive TAG biosynthesis systems, the ^{13}C isotopomer patterns indicate differences in central carbon metabolism (Fig. 9). In system A, exogenous glycerol is mainly used for glyceryl labeling, with only a very small mole fraction, if any, routed to acyl labeling. The endogenous G3P supply is almost completely inhibited. Estimates for the contribution of endogenous [$^{12}C_3$]glyceryl are of the order of 0 to 1 mol per 9.5 mol of [$^{13}C_3$]glyceryl, that is, ≤10 mol%. In system B, the mole fraction of glycerol diverted to acyl labeling is greater than that utilized for lipid glyceryl labeling, the molar ratio being approximately 2 to 1. Furthermore, estimates for the molar contribution of endogenous [$^{12}C_3$]glyceryl to [$^{13}C_3$]glyceryl are about 2:1 to 3:1, the converse of system A.

The high level of glyceryl labeling from exogenous glycerol in cultured Camelina embryos was previously discussed in terms of efficient glycerol activation by a kinase to G3P and the effect of this new source of G3P on the endogenous G3P dehydrogenase reactions that utilize dihydroxyacetone phosphate (24). The G3P dehydrogenase reaction was inferred to be far from equilibrium and G3P to be an allosteric or competitive inhibitor. There are plastid, cytosol, and mitochondrial outer envelope isoforms of G3P dehydrogenase in the plant cell, and multiple genes, such that differential enzyme kinetics, could play an important role in the distribution of (M + 3) *versus* (M + 2) and (M + 5) labeling in systems A and B. There is, however, an alternative explanation that might add to or replace this hypothesis. At ambient light in the Camelina seed, the embryo has low carbon conversion efficiency (∼32%) (22). By comparison, rapeseed and Arabidopsis embryos have efficiencies of ∼80%. Metabolic flux analysis suggests that this reduced efficiency in Camelina is caused by a massive plastid oxidative pentose pathway flux. If such a flux was localized solely to system A, then both system A and B could exhibit similar G3P dehydrogenase back reactions to generate triose phosphates from G3P. But in system A, the highly active oxidative pentose phosphate pathway would convert most of this label from exogenous glycerol to carbon dioxide, thus greatly reducing (M + 2) and (M + 5) labeling in system A.

A third possible explanation, elaborated in the final paragraph of the Discussion section, invokes the unique function of the epidermis for the synthesis of extracellular lipids.

The presence of different systems of TAG synthesis within Camelina embryos requires explanation. Separate systems operating together in the same cell would require complex metabolic partitioning by compartmentation and/or channeling. Plastid and cytoplasmic glycerolipid assembly cannot define A and B, as both depend on plastid *de novo* fatty acid synthesis, and so would have similar acyl labeling contributions from glycerol. Discounting these types of explanations leaves those based on tissue and cell types, including possible differential development of such tissue layers and/or cells. Prior observations suggest several options for the location of distinct TAG synthesis systems. These include different levels of VLCFA in axis and cotyledons (25), differential development of the inner and outer cotyledons (27), and the known cellular organization within the embryo (29). These options are reviewed with respect to TAG ^{13}C isotopomer distributions measured in either dissected parts of the embryo or from differential solvent extraction.

TAG in the axis of mature Camelina embryos contains little VLCFA; the opposite occurs in cotyledons (25). This holds true for 16 DPA embryos, as confirmed by TAG acyl carbon molecular species analysis (Fig. 7), and by fatty acid analysis, which showed VLCFA content in total lipids to be almost twofold higher in cotyledons (Fig. S10). A simple compositional analysis suggested C34-DAG was primarily acylated by C18 (+C16) fatty acids to produce TAG, whereas C38-DAG was primarily acylated by VLCFA. C36-DAG showed an intermediate acylation preference (Fig. 1). Thus, the synthesis of TAG from C34-DAG and C36-DAG by preferential acylation with C16 and C18 fatty acids and from C36-DAG and C38-DAG by acylation with VLCFA reports metabolism dominating in different parts of the embryo. The relative FAE1 gene expression, protein levels, and enzyme activity in the two tissues are unknown. When axis and cotyledons are compared for their TAG ^{13}C isotopomer profiles, these are essentially identical (Table 3). Thus, system A and B isotopomer distributions are independent of the modulation of FAE1-based metabolism. Confirmation of this conclusion can be found in Figure S12. The individual TAGs (C52–C58) have similar patterns of (M + 3) *versus* (M + 2) and (M + 5) kinetics, even though there are small differences in relative contributions. Thus, the phenomenon of A and B systems is not simply a function of or correlation with TAG acyl carbon number. Another explanation must be found.

Another possibility arises from the observation in oilseed rape that the inner cotyledon lags in development and storage product accumulation compared with the axis and outer cotyledon (27). The proposed driving force for this differential development is that the axis and outer cotyledon exhibit largely photoheterotrophic growth, whereas the inner cotyledon exhibits a greater degree of heterotrophic growth, with the difference caused by seed architecture. In the cultured embryo system, such constraints are removed (Fig. S9). However, the lipid biosynthetic heterogeneity persists, and at the time of assay, the inner cotyledons are smaller and contain about half the lipid of the outer cotyledons (Table S3). The fact that the inner and outer cotyledons exhibit similar TAG ^{13}C isotopomer profiles suggests that this difference is not the major determinant producing systems A and B. Figure 8, panel *C*, shows that for the whole embryo, (M + 2) isotopomer is highest in C56-TAGs and C58-TAGs. As noted earlier (Fig. S2), unlike acetate, glycerol does not preferential label the acetyl-CoA pool used by the cytosolic FAE1 system, so this is not a cause of the preferential (M + 2) isotopomer labeling of C56-TAGs and C58-TAGs. The data in Table 3 confirm this TAG (M + 2) molecular species enrichment pattern and show that it is seen across all three tissues. Thus, systems A and B cannot be attributed to developmental or other differences between the inner and outer cotyledons. If TAG (M + 2) isotopomers arose specifically in the inner cotyledon, it would be expected that the TAG profile would mirror the isotopomer distribution, with C58 $\sim$ C56 $>$ C54 $>$ C52. But this is not the TAG mass composition of the inner cotyledon. Inner and outer cotyledons have similar mass distributions, namely C56 $>$ C54 $>>$ C58 $\sim$ C52.

Embryos consist of multiple cell types, most or all of which must be TAG rich to account for the high oil content found in *C. sativa* embryos, peaking at 47% of dry weight in culture (23). As the ^{13}C isotopomers corresponding to systems A and B are present at equivalent levels across inner and outer cotyledons and the axis, one plausible explanation would be that the kinetically defined distinct lipid synthesis systems are located in different cell layers common to these parts. To further investigate this possibility, differential extraction of lipids from intact embryos was attempted. This must be distinguished from rapid tissue dipping protocols used for obtaining surface waxes and exudates (40). Differential extraction of internal lipids from plants has apparently not been reported previously. There are no known internal controls, and the situation is complicated because a number of physical parameters are unknown or likely to be heterogeneous. Briefly, these may include heterogeneity of cell wall porosity, the unknown rates of penetration of solvent into the tissue and back diffusion of water, different TAG extraction rates from oil bodies and membranes, and the possibility that lipid mixing within tissues may be substantially faster than diffusion from the tissue to the bulk solvent. Despite these, discriminations between rates of ^{13}C isotopomer extraction were observed, and even though lipid extraction kinetics appeared to be a low-resolution method, it is reasonable to assume that cell layer depth is at least one primary determinant. Thus, the observation that (M + 2) and (M + 5) TAG isotopomers are preferentially extracted from intact embryos over (M + 3) TAG isotopomers (Fig. 8) is taken as evidence that the former are likely to be associated with the surface layer(s).

Biological implications for lipid rate and pool size determinations and two TAG synthesis systems

The accumulation of mature oil bodies in developing seeds requires PL for the half unit membrane surrounding the

neutral lipid core. There is an inverse relationship between oil body diameter and the amount of PL (9). Oil bodies in seeds typically range between 0.5 and 2.5 μm in average diameter, with PL content of 2.5 to 0.5 mass percent, respectively. Data are not available for *C. sativa*, but various *Brassica* species have oil bodies reported in the range of 0.65 to 0.75 μm, equivalent to 2 to 1.6 w % PL (41), whereas *Arabidopsis thaliana* (Col-0) has oil bodies of 1.7 μm diameter, equivalent to 0.8 w % PL (42). Since glyceryl labeling indicates PL accumulation at 12 mol% (Table 1), this is likely to be many fold over that required for oil body assembly. Another large-scale membrane proliferation process in these cells is likely to involve storage protein body formation. However, no data are apparently available on net membrane lipid biosynthesis for that process.

It would be expected that active and inactive PC pools (or membrane domains) will share the same cells. Active domains might include the endoplasmic reticulum and possibly the oil-body–associated half-unit membrane (9); inactive domains might include the outer leaflet of plastid envelope, the inner leaflet of the plasma membrane, and membranes bounding mitochondria, tonoplast, and peroxisomes. The fact that the inactive DAG and PC pools are about 70% of the total rules out a distinction between inner and outer leaflets of membranes as the only explanation: however, that part of the inactive pool might represent that the inner leaflet of membranes remains a partial explanation, especially since the vectorial nature of TAG synthesis enzymes is still poorly understood.

In this and the previous section, quantitative consideration has been given to the rate of TAG synthesis, the intermediate pool that provides for system A ((M + 3)TAG), and the size of the major components of this pool, namely DAG and PC, that provide for this major flux. The results provide values for the embryo at midmaturation (16 DPA). As TAG synthesis rates increases with time in culture, these active pool sizes will most likely increase. The optimum simulation described in Figure 5 to fit the measured TAG [$^{13}C_3$*glyceryl*]-specific activity began with [$^{12}C_3$*glyceryl*] contribution of 0.2 mol per mol of [$^{13}C_3$*glyceryl*], but this was increased to 0.6 mol after 15 h in culture, then to 1.2 mol at 45 h in culture. The exactness of the fit is of less importance than the fact that there is increasing dilution of ^{13}C label over time. As most of the [$^{13}C_3$*glyceryl*] DAG and PL provide for the (M + 3)TAG intermediate pool, it is expected that the DAG and PL accumulations will also increase commensurately. The degree to which they contribute to the active pool remains to be determined. What can be clearly stated for system A, given the results from precursor–product kinetics and mole fraction analysis, is that its TAG synthesis requires that there is only a single intermediate pool that encompasses a large fraction of total membrane lipids. Thus, there is no complete *de novo* glycerolipid synthesis metabolon for TAG synthesis, that is, contiguous from the initial *sn*-1 acylation to the final *sn*-3 acylation. This does not rule out some specific enzyme–enzyme interactions to give localized metabolic channeling. This kinetic study does not have adequate resolution on this question concerning system B. Also, for system B components, the intermediate time course gives (M + 2) > (M + 5) for TAG isotopomers (Fig. 6*B*), whereas the long-term time course shows (M + 5) > (M + 2) for TAG isotopomers (Fig. S4*C*). Other differences between the time courses have already been noted. Over extended culture, the net lipid synthesis rate increases twofold to threefold, but the continuous increases of both (M + 2) and (M + 5) TAG isotopomers argues that system B is persistent, even if the balance between isotopomers can be modulated.

For Camelina embryos, there are no anatomical depictions at cellular resolution of developing or mature embryos, such as are available for Arabidopsis embryos (29). Nor were we able to find published electron micrographs from any seed clearly identifying oil bodies in the embryo epidermis. Thus, it is not possible to make any accurate determination of the TAG content of the epidermal layer. Nevertheless, given the size of a Camelina embryo, taking a surface cell layer as 20 to 40 μm deep, considering the high surface area to volume ratio of the embryo and assuming epidermal cell oil content per unit volume is similar to that of the bulk tissue, then the epidermal layer might contain 20 to 25% of the total embryo lipid. This is consistent with the hypothesis that system B could represent the epidermal layer. Furthermore, the epidermis will contain cells destined to become epidermal pavement cells, trichome cells, and stomata. Thus, "system B" itself may contain a rather heterogeneous collection of lipid biosynthesis types. Surface cells are unique lipid biosynthesis systems, with a specialist function, in addition to basal lipid metabolism, largely to sustain extracellular lipid metabolism, namely cutin and suberin synthesis and associated waxes (40, 43, 44), and in rarer cases, surface glycerolipids (45, 46). This includes acylglycerol synthesis and transport, with the possibility of extracellular transacylation producing glycerol for recycling. This might engender the back reaction for the G3P dehydrogenase reaction. Thus, a distinctive TAG synthesis system in such a layer of cells would not be unexpected. The more general point is that the hypothesis that system B represents the epidermal layer is the most obvious for further experimental exploration.

Conclusions

Culturing developing *C. sativa* embryos with exogenous glycerol labels a large mole fraction of total glyceryl groups in lipid biosynthesis, with a smaller contribution to acyl group labeling. Tracking ^{13}C labeling with MS offers an advantage over ^{14}C labeling in that acyl and glyceryl connectivities can be determined. This allowed detection of two TAG synthesis systems. The systems differ in their TAG synthesis kinetics, in the metabolism of exogenous glycerol, and in their contribution to total lipid biosynthetic flux. The finding of separate systems was unexpected. The quantitative kinetic description of the major flux pathway provided rate and intermediate pool size data, and the absolute mole fraction for the major intermediates DAG and PC relative to total embryo amounts. These values are for midmaturation embryos and will likely vary with seed development. Evidence was provided to support the hypothesis that the system with the lower flux contribution, and which has a very small intermediate pool, was likely a

surface layer(s) extending across the entire embryo. Additional localization methods are required to confirm and refine this description. Future experiments to define the lipid flux network in developing oilseeds will have to take *de novo* TAG synthesis heterogeneity into account. Different cellular systems and sizes of intermediate lipid pools may influence the relative contribution of DGAT and transacylases, such as PDAT, in TAG synthesis. This will have biotechnology ramifications for producing seed oils with enhanced oil content and composition.

Experimental procedures

Many of the methods are described in detail in previous references (23, 24). These include protocols for plant growth, embryo culture, assays for lipid biosynthesis, lipid analysis including TLC and hydrogenation, and ^{14}C and ^{13}C fatty acid and lipid analysis. An outline of these methods is provided here, along with salient new features. Additional information is given in the supporting information for Experimental procedures section under "Supplemental text for ^{13}C isotopomer analysis" and accompanying Figures S1–S4, S9, and S13.

Plant materials, embryo culture, and embryo assays

Siliques from wildtype *C. sativa* plants, var. Sunesson, grown in a growth chamber, were harvested at 15 DPA. Embryos were dissected aseptically from the developing seeds and placed in culture (five embryos per well, in 1.0 ml culture medium). After overnight, culture assays were initiated using ^{14}C and/or ^{13}C substrates in culture medium (0.5 ml added/well). The embryos are thus assayed at 16 DPA. For the kinetic time courses, embryos from two wells were pooled per assay. The standard assay contained 2 mM [$^{13}C_3$]glycerol (Aldrich; 489476, 99 atom %) plus [U-^{14}C]glycerol (PerkinElmer; NEC441X, 141 Ci/mol, 6.35 μCi), a saturating concentration for lipid biosynthesis. After the allotted incubation time, the medium was removed, the embryos quickly washed with deionization water, and heated at 80 to 85 °C in isopropanol for 10 to 15 min to inactivate lipases prior to lipid extraction. Lipids were extracted with hexane–isopropanol according to the method of Hara and Radin (47). Tripentadecanoin was added during tissue grinding and extraction as an internal standard.

^{14}C lipid analyses

Aliquots of the total lipid extract were assayed for radioactivity by liquid scintillation counting. Neutral lipids were analyzed on silica TLC plates developed with 88/12 (v/v) toluene/ethyl acetate. PLs were analyzed on silica TLC plates developed with 85/15/5/2 (v/v/v/v) chloroform/methanol/acetic acid/water. The ^{14}C TLC plates were subject to autoradiography using Kodak Phosphor Screens GP. After exposure, the screens were scanned using the Bio-Rad PMI FX phosphoimager, and radioactivity bands were quantified using Bio-Rad Quantity One basic software. Scanning TLC plates by radiometric or phosphor imaging systems can introduce bias when comparing different lipid classes, and especially when comparing neutral with PLs (Fig. S13). The appropriate controls, that is, scrapping and liquid scintillation counting of representative lipid TLC bands, were included to correct for this bias. Measurement of the distribution of label from [$^{14}C_3$] glycerol into [$^{14}C_3$*glyceryl*] and/or [$^{14}C_2$*acyl*] lipid is described in Figure S4.

Analysis of ^{13}C lipid isotopomer distributions

An aliquot of the total lipid extract was hydrogenated, and the resulting saturated total lipid sample was fractionated by preparative silica TLC. TAG, the combined αα-DAG and αβ-DAG, and PC bands were eluted from the silica. The combined αα-DAG and αβ-DAG was acetylated with acetic anhydride–pyridine. The hydrogenated TAGs, ac-DAGs, and PC were analyzed by ESI–MS in positive ion mode, using a Waters Acquity UPLC autosampler coupled to a Waters Quattro Micro mass spectrometer. Sample solutions (10 μl) were introduced into the electrospray source by flow injection into a 97:3 isopropanol:10 mM aqueous ammonium acetate buffer flowing at 0.1 ml/min. The capillary and extractor voltages were 3.2 kV and 2.0 V, respectively. Mass spectra were collected for 2 min; the m/z range scanned in the MS measurements was from 500 to 1000 (1 s/scan). Mass spectra data were acquired with MassLynx 4.0 software (Waters Corp). Technical replicates were run in triplicate. Included were replicates of saturated TAG, ac-DAG, or PC standard mixtures. These had Cn ranges overlapping with those of the biological samples and total concentrations similar to the biological samples.

The steps for the calculation of TAG, DAG, and PC biosynthetically derived isotopomer profiles are described graphically in Figure S3 using a worked example. For each Cn molecular species within a lipid class, the isotopomer profile will differ. The standard mixture for each lipid class permits the calculation of relative molar response factors, which are then applied to the biological sample C(n + 2) molecular species. Thus, for the lipid class, the average mole fraction for each isotopomer was calculated from the sum of isotopic mole fraction multiplied by the mass mole fraction over all molecular species.

Measuring variations of TAG isotopomer distributions within different tissues and by differential solvent extraction

For a comparison of isotopomer distributions in TAG, cultured embryos were incubated for 4 h with 2 mM [$^{13}C_3$] glycerol as substrate but without ^{14}C tracer. For the dissection of tissues, 24 embryos were pooled per assay. The embryos were then transferred to a dissecting microscope stage, still in culture medium, and dissected into axis, inner cotyledon, and outer cotyledon tissues. These were kept on the stage, with residual assay medium, and after the dissections, which took about 30 min, each tissue set was transferred to a culture tube for hot isopropanol quenching at the same time. Thus, the tissues were actually in contact with substrate for about 4.5 h. The dissection of inner and outer cotyledons and axis in cultured embryos is described in Figure S9.

To undertake differential lipid extraction of intact and cultured lipids, two solvent systems were first tested. Time courses for extraction were run with 95:5 (v/v) isopropanol–water at 80 °C and with 20/10/1 (v/v/v) chloroform–methanol–water at room temperature. Despite being at a significantly lower temperature, the chloroform–methanol–water system exhibited more rapid lipid extraction. Assays of 36 pooled embryos were extracted intact with 4 ml 20/10/1 (v/v/v) chloroform–methanol–water at room temperature for successive periods of 10, 20, and 40 min, with occasional mixing. The embryos were then quenched in hot isopropanol, ground, and the remaining lipid extracted with hexane–isopropanol.

For both the dissection and extraction kinetics experiments, the total lipid extracts were first hydrogenated. An aliquot was transmethylated to assess acyl recoveries, and the remainder subjected to preparative TLC, with TAG quantification and ^{13}C isotopomer analysis by ESI–MS.

Data availability

All data for this study are included in the article and/or supporting information.

Supporting information—This article contains supporting information (48–50).

Acknowledgments—We thank Danielle Delamarter for technical assistance with plant growth, embryo culture, and lipid extractions, and Dr Tony Schilmiller and the Michigan State University Research Technology Support Facility, Mass Spectrometry, and Metabolomics Core for technical support and MS instrumentation. This research was supported by the Office of Science (BER), US Department of Energy, grant no DE-SC0018269.

Author contributions—M. P. and Y. S.-H. conceptualization; M. P. methodology; M. P. validation; M. P. formal analysis; M. P. investigation; M. P. writing–original draft; M. P. and Y. S.-H. writing–review and editing; M. P. visualization; Y. S.-H. funding acquisition.

Funding and additional information—M. P. received no salary funding during this research.

Conflict of interest—The authors declare that they have no conflicts of interest with the contents of this article.

Abbreviations—The abbreviations used are: DAG, diacylglycerol; DGAT, diacylglycerol acyltransferase; DPA, days post anthesis; ESI, electrospray ionization; FAE, fatty acyl-CoA elongase; GL, galactolipid; G3P, glycerol-3-phosphate; PC, phosphatidylcholine; PDAT, phospholipid diacylglycerol acyltransferase; PE, phosphatidylethanolamine; PG, phosphatidylglycerol; PI, phosphatidylinositol; PL, polar lipid; TAG, triacylglycerol; VLCFA, very long-chain fatty acid.

References

1. Mubofu, E. B. (2016) Castor oil as a potential renewable resource for the production of functional materials. *Sustainable Chem. Process.* **4**, 11
2. Usher, S., Han, L., Haslam, R. P., Michaelson, L. V., Sturtevant, D., Aziz, M., Chapman, K. D., Sayanova, O., and Napier, J. A. (2017) Tailoring seed oil composition in the real world: Optimizing omega-3 long chain polyunsaturated fatty acid accumulation in transgenic *Camelina sativa*. *Nat. Sci. Rep.* **7**, 6570
3. Aznar-Moreno, J. A., and Durrett, T. D. (2017) Review: Metabolic engineering of unusual lipids in the synthetic biology era. *Plant Sci.* **263**, 126–131
4. Bates, P. D., Stymne, S., and Ohlrogge, J. (2013) Biochemical pathways in seed oil synthesis. *Curr. Opin. Plant Biol.* **16**, 358–364
5. Malik, M. R., Tang, J., Sharma, N., Burkitt, C., Ji, Y., Mykytyshyn, M., Bohmert-Tatarev, K., Peoples, O., and Snell, K. D. (2018) Camelina sativa, an oilseed at the nexus between model system and commercial crop. *Plant Cell Rep.* **37**, 1367–1381
6. Napier, J. A., Haslam, R. P., Beaudoin, F., and Cahoon, E. B. (2014) Understanding and manipulating plant lipid composition: Metabolic engineering leads the way. *Curr. Opin. Plant Biol.* **19**, 68–75
7. Baud, S., and Lepiniec, L. (2010) Physiological and developmental regulation of seed oil production. *Prog. Lipid Res.* **49**, 235–249
8. Li-Beisson, Y., Shorrosh, B., Beisson, F., Andersson, M. X., Arondel, V., Bates, P. D., Baud, S., Bird, D., Debono, A., Durrett, T. P., Franke, R. B., Graham, I. A., Katayama, K., Kelly, A. A., Larson, T., *et al.* (2013) Acyl-lipid metabolism. *Arabidopsis Book* **11**, e0161
9. Huang, A. H. C. (1992) Oil bodies and oleosins in seeds. *Annu. Rev. Plant Physiol. Plant Mol. Biol.* **43**, 177–200
10. Bates, P. D., Durrett, T. P., Ohlrogge, J. B., and Pollard, M. (2009) Analysis of acyl fluxes through multiple pathways of triacylglycerol synthesis in developing soybean embryos. *Plant Physiol.* **150**, 55–72
11. Coleman, R. A. (2019) It takes a village: Channeling fatty acid metabolism and triacylglycerol formation *via* protein interactomes. *J. Lipid Res.* **60**, 490–497
12. Zhang, Y., and Fernie, A. R. (2021) Metabolons, enzyme–enzyme assemblies that mediate substrate channeling, and their roles in plant metabolism. *Plant Commun.* **2**, 100081
13. Xu, Y., Caldo, K. M. P., Jayawardhane, K., Ozga, J. A., Weselake, R. J., and Chen, G. (2019) A transferase interactome that may facilitate channeling of polyunsaturated fatty acid moieties from phosphatidylcholine to triacylglycerol. *J. Biol. Chem.* **294**, 14838–14844
14. Regmi, A., Shockey, J., Kotapati, H. K., and Bates, P. D. (2020) Oil-producing metabolons containing DGAT1 use separate substrate pools from those containing DGAT2 or PDAT. *Plant Physiol.* **184**, 720–737
15. An, D., and Suh, M.-C. (2015) Overexpression of Arabidopsis WRI1 enhanced seed mass and storage oil content in *Camelina sativa*. *Plant Biotechnol. Rep.* **9**, 137–148
16. Bansal, S., and Durrett, T. P. (2016) *Camelina sativa:* An ideal platform for the metabolic engineering and field production of industrial lipids. *Biochimie* **120**, 9–16
17. Chhikara, S., Abdullah, A. M., Akbari, P., Schnell, D., and Dhankher, O. P. (2018) Engineering *Camelina sativa* (L.) Crantz for enhanced oil and seed yields by combining diacylglycerol acyltransferase1 and glycerol-3-phosphate dehydrogenase expression. *Plant Biotechnol. J.* **16**, 1034–1045
18. Dalal, J., Lopez, H., Vasani, N. B., Hu, Z., Swift, J. E., Yalamanchili, R., Dvora, M., Lin, X., Xie, D., Qu, R., and Sederoff, H. W. (2015) A photorespiratory bypass increases plant growth and seed yield in biofuel crop *Camelina sativa*. *Biotechnol. Biofuels* **8**, 175
19. Yuan, L., and Li, R. (2020) Metabolic engineering a model oilseed *Camelina sativa* for the sustainable production of high-value designed oils. *Front. Plant Sci.* **11**, 11
20. Klinska, S., Jasieniecka-Gazarkiewicz, K., and Banas, A. (2019) Acyl-CoA: lysophosphatidyl-choline acyltransferases (LPCATs) of *Camelina sativa* seeds: Biochemical properties and function. *Planta* **250**, 1655–1670
21. Lager, I., Jeppson, S., Gippert, A.-L., Feussner, I., Stymne, S., and Marmon, S. (2020) Acyltransferases regulate oil quality in *Camelina sativa* through both acyl donor and acyl acceptor specificities. *Front. Plant Sci.* **11**, 1144
22. Carey, L. M., Clark, T. J., Deshpande, R. R., Cocuron, J.-C., Rustad, E. K., and Shachar-Hill, Y. (2020) High flux through the oxidative pentose phosphate pathway lowers efficiency in developing Camelina seeds. *Plant Physiol.* **182**, 493–506

23. Pollard, M., Martin, T. M., and Shachar-Hill, Y. (2015) Lipid analysis of developing *Camelina sativa* seeds and cultured embryos. *Phytochemistry* **118**, 23–32
24. Pollard, M., Delamarter, D., Martin, T. M., and Shachar-Hill, Y. (2015) Lipid labeling from acetate or glycerol in cultured embryos of *Camelina sativa* seeds: A tale of two substrates. *Phytochemistry* **118**, 192–203
25. Horn, P. J., Silva, J. E., Anderson, D., Fuchs, J., Borisjuk, L., Nazarenus, T. J., Shulaev, V., Cahoon, E. B., and Chapman, K. D. (2013) Imaging heterogeneity of membrane and storage lipids in transgenic Camelina sativa seeds with altered fatty acid profiles. *Plant J.* **76**, 138–150
26. Millar, A. A., and Kunst, L. (1997) Very-long-chain fatty acid biosynthesis is controlled through the expression and specificity of the condensing enzyme. *Plant J.* **12**, 121–131
27. Borisjuk, L., Neuberger, T., Schwender, J., Heinzel, N., Sunderhaus, S., Fuchs, J., Hay, J. O., Tschiersch, H., Braun, H.-P., Denolf, P., Lambert, B., Jakob, P. M., and Rolletschek, H. (2013) Seed architecture shapes embryo metabolism in oilseed rape. *Plant Cell* **25**, 1625–1640
28. Li, Y., Beisson, F., Pollard, M., and Ohlrogge, J. (2006) Oil content of Arabidopsis seeds: The influence of seed anatomy, light and plant-to-plant variation. *Phytochemistry* **67**, 904–915
29. Bassel, G. W., Stamma, P., Moscab, G., Barbier de Reuille, P., Gibbs, D. J., Winter, R., Janka, A., Holdsworth, M. J., and Smith, R. S. (2014) Mechanical constraints imposed by 3D cellular geometry and arrangement modulate growth patterns in the Arabidopsis embryo. *Proc. Natl. Acad. Sci. U. S. A.* **111**, 8685–8690
30. Slack, R., Roughan, P. G., and Balasingham, N. (1978) Labeling of glycerolipids in the cotyledons of developing oilseeds by [1-^{14}C]acetate and [2-^{3}H]glycerol. *Biochem. J.* **170**, 421–433
31. Allen, D. K., Libourel, I. G. L., and Shachar-Hill, Y. (2009) Metabolic flux analysis in plants: Coping with complexity. *Plant Cell Environ.* **32**, 1241–1257
32. Slack, C. R., Roughan, P. G., and Balasingham, N. (1977) Labeling studies *in vivo* on metabolism of acyl and glycerol moieties of glycerolipids in developing maize leaf. *Biochem. J.* **162**, 289–296
33. Slack, C. R., Campbell, L. C., Browse, J. A., and Roughan, P. G. (1983) Some evidence for the reversibility of the cholinephosphotransferase-catalyzed reaction in developing linseed cotyledons *in vivo*. *Biochim. Biophys. Acta* **754**, 10–20
34. Slack, C. R., Roughan, P. G., Browse, J. A., and Gardiner, S. E. (1985) Some properties of cholinephosphotransferase from developing safflower cotyledons. *Biochim. Biophys. Acta* **833**, 438–448
35. Stobart, A. K., and Stymne, S. (1985) The interconversion of diacylglycerol and phosphatidylcholine during triacylglycerol production in microsomal preparations of developing cotyledons of safflower (Carthamus tinctorius L.). *Biochem. J.* **232**, 217–221
36. Lu, C., Xina, Z., Ren, Z., Miquel, M., and Browse, J. (2009) An enzyme regulating triacylglycerol composition is encoded by the ROD1 gene of Arabidopsis. *Proc. Natl. Acad. Sci. U. S. A.* **106**, 18837–18842
37. Ohlrogge, J. B., Pollard, M. R., and Stumpf, P. K. (1978) Studies on biosynthesis of waxes by developing jojoba seed tissue. *Lipids* **13**, 203–210
38. Pollard, M. R., and Stumpf, P. K. (1980) Long chain (C20 and C22) fatty acid biosynthesis in developing seeds of *Tropaeolum majus*: An *in vivo* study. *Plant Physiol.* **66**, 641–648
39. Pollard, M. R., and Stumpf, P. K. (1980) Biosynthesis of C20 and C22 fatty acids by developing seeds of *Limnanthes alba*: Chain elongation and delta-5 desaturation. *Plant Physiol.* **66**, 649–655
40. Razeq, F. M., Kosma, D. K., Rowland, O., and Molina, I. (2014) Extracellular lipids of *Camelina sativa*: Characterization of chloroform-extractable waxes from aerial and subterranean surfaces. *Phytochemistry* **106**, 188–196
41. Tzen, J. T. C., Cao, Y.-Z., Laurent, P., Ratnayake, C., and Huang, A. H. C. (1993) Lipids, proteins, and structure of seed oil bodies from diverse species. *Plant Physiol.* **101**, 267–276
42. Wang, F., Zheng, T., Hu, Z., Wu, G., Lang, C., and Liu, R. (2020) Overexpression of miR319a altered oil body morphogenesis and lipid content in Arabidopsis seeds. *Plant Mol. Biol. Rep.* **38**, 531–537
43. Beisson, F., Li-Beisson, Y., and Pollard, M. (2012) Solving the puzzles of cutin and suberin polymer biosynthesis. *Curr. Opin. Plant Biol.* **15**, 329–337
44. Razeq, F. M., Kosma, D. K., França, D., Rowland, O., and Molina, I. (2021) Extracellular lipids of *Camelina sativa*: Characterization of cutin and suberin reveals typical polyester monomers and unusual dicarboxylic fatty acids. *Phytochemistry* **184**, 112665
45. Matsuzaki, T., Koiwai, A., and Kawashima, N. (1983) Changes in stigma-specific lipids of tobacco plant during flower development. *Plant Cell Physiol.* **24**, 207–213
46. Simpson, J. P., and Ohlrogge, J. B. (2016) A novel pathway for triacylglycerol biosynthesis is responsible for the accumulation of massive quantities of glycerolipids in the surface wax of Bayberry (*Myrica pensylvanica*) fruit. *Plant Cell* **28**, 248–264
47. Hara, A., and Radin, N. S. (1978) Lipid extraction of tissues with a low-toxicity solvent. *Anal. Biochem.* **90**, 420–426
48. Ichihara, K., Shibahara, A., Yamamoto, K., and Nakayama, T. (1996) An improved method for rapid analysis of the fatty acids of glycerolipids. *Lipids* **31**, 535–539, 48
49. Bannon, C. D., Craske, J. D., and Hillker, A. E. (1986) Analysis of fatty acid methyl esters with high accuracy and reliability. V. Validation of theoretical relative response factors of unsaturated esters in the flame ionization detector. *J. Amer. Oil Chem. Soc.* **63**, 105–110, 49
50. Craske, J. D., and Bannon, C. D. (1987) Gas liquid chromatography analysis of the fatty acid composition of fats and oils: a total system for high accuracy. *J. Amer. Oil Chem. Soc.* **64**, 1413–1417